

Mapping Pharmacologically-induced Functional Reorganisation onto the Brain's Neurotransmitter Landscape

Andrea I. Luppi^{1,2,3,4*}, Justine Y. Hansen⁵, Ram Adapa¹, Robin L. Carhart-Harris⁶, Leor Roseman⁷, Daniel Golkowski⁸, Andreas Ranft⁹, Rüdiger Ilg^{8,10}, Denis Jordan¹¹, Alexander R. D. Peattie^{1,2}, Anne E. Manktelow¹, Draulio B. de Araujo¹², Stefano L. Sensi^{13,14}, Adrian M. Owen¹⁵, Lorina Naci¹⁶, David K. Menon^{1,17}, Bratislav Misic⁵, Emmanuel A. Stamatakis^{1,2}

¹Division of Anaesthesia, University of Cambridge, Cambridge, UK.

²Department of Clinical Neurosciences, University of Cambridge, Cambridge, UK.

³Leverhulme Centre for the Future of Intelligence, University of Cambridge, Cambridge, UK.

⁴The Alan Turing Institute, London, UK.

⁵McConnell Brain Imaging Center, Montreal Neurological Institute, McGill University, Montreal, QC, Canada.

⁶Psychedelics Division - Neuroscape, Department of Neurology, University of California San Francisco, San Francisco, CA, USA.

⁷Center for Psychedelic Research, Department of Brain Sciences, Imperial College London, London, UK.

⁸Department of Neurology, Klinikum rechts der Isar, Technical University Munich, München, Germany.

⁹Technical University of Munich, School of Medicine, Department of Anesthesiology and Intensive Care, Munich, Germany.

¹⁰Asklepios Clinic, Department of Neurology, Bad Tölz, Germany.

¹¹Department of Anaesthesiology and Intensive Care Medicine, Klinikum rechts der Isar, Technical University Munich, München, Germany.

¹²Department of Neuroscience and Imaging and Clinical Science, Center for Advanced Studies and Technology, Institute for Advanced Biomedical Technologies, University "G. d'Annunzio" Chieti-Pescara, Chieti, Italy.

¹³Institute for Memory Impairments and Neurological Disorders, University of California-Irvine, Irvine, CA, USA.

¹⁴Brain Institute, Federal University of Rio Grande do Norte, Natal, RN, Brazil.

¹⁵Department of Psychology and Department of Physiology and Pharmacology, The Brain and Mind Institute, Western University, London, ON, Canada.

¹⁶Trinity College Institute of Neuroscience, School of Psychology, Trinity College Dublin, Dublin, Ireland.

¹⁷Wolfson Brain Imaging Centre, University of Cambridge, Cambridge, UK.

Corresponding author: email: al857@cam.ac.uk

Abstract

58
59
60
61
62
63
64
65
66
67
68
69
70
71
72
73
74
75
76
77
78
79
80

To understand how pharmacological interventions can exert their powerful effects on brain function, we need to understand how they engage the brain's rich neurotransmitter landscape. Here, we bridge microscale molecular chemoarchitecture and pharmacologically-induced macroscale functional reorganisation, by relating the regional distribution of 18 neurotransmitter receptors and transporters obtained from Positron Emission Tomography, and the regional changes in functional MRI connectivity induced by 7 different mind-altering drugs including anaesthetics, psychedelics, and cognitive enhancers. Our results reveal that psychoactive drugs exert their effects on brain function by engaging multiple neurotransmitter systems. Intriguingly, the effects of both anaesthetics and psychedelics on brain function, though opposite, are organised along hierarchical gradients of brain structure and function. Finally, we show that regional co-susceptibility to pharmacological interventions recapitulates co-susceptibility to disorder-induced structural alterations. Collectively, these results highlight rich statistical patterns relating molecular chemoarchitecture and drug-induced reorganisation of the brain's functional architecture.

Keywords: PET; receptors; neurotransmitters; functional MRI; pharmacology; anaesthesia; psychedelic; cognitive enhancer

81 Introduction

82 Understanding how the brain orchestrates complex signals across spatial and
83 temporal scales to support cognition and consciousness is a fundamental challenge
84 of contemporary neuroscience. By inducing profound but reversible alterations of
85 brain function, psychoactive compounds provide neuroscientists with the means to
86 manipulate the brain without requiring surgical intervention. In combination with non-
87 invasive brain imaging techniques such as functional MRI, acute pharmacological
88 interventions have therefore emerged as a prominent tool for causal investigation of
89 the relationship between brain and cognitive function in healthy humans ¹.

90

91 Mind-altering pharmacological agents also play a fundamental role in modern clinical
92 practice. The invention of anaesthesia was a major milestone in medical history,
93 enabling millions of life-saving surgeries to take place every year ². Other drugs that
94 influence the mind without suppressing consciousness, such as the cognitive
95 enhancers modafinil and methylphenidate, have found useful applications in
96 alleviating the cognitive symptoms of syndromes such as ADHD, narcolepsy, and
97 traumatic brain injury (TBI) ³⁻¹¹. More recently, classic and “atypical” psychedelics
98 are increasingly being investigated for their potential to provide breakthrough
99 avenues to treat psychiatric conditions, with recent successes in clinical trials
100 heralding a possible end to the current scarcity of therapies for treatment-resistant
101 depression and other neuropsychiatric disorders ¹²⁻¹⁷. For these convergent reasons,
102 the effects of anaesthetics, psychedelics, and cognitive enhancers on brain function
103 are becoming the focus of intense investigation, revealing both similarities and
104 differences between them ¹⁸⁻²⁶.

105 Pharmacological agents exert their mind-altering effects by tuning the brain’s
106 neurotransmitter landscape. Neurotransmitters engage receptors on neurons’
107 membrane to mediate the transfer and propagation of signals between cells,
108 modulate the functional configurations of neuronal circuits, and ultimately shape
109 network-wide communication ²⁷⁻³¹. Several psychoactive drugs appear to exert their
110 effects on the mind and brain primarily through one or few specific neurotransmitters:
111 the main action of the general anaesthetic propofol is enhancement of synaptic
112 transmission mediated by GABA-A receptors, a mechanism that is also shared by

113 sevoflurane, which in addition attenuates glutamatergic synaptic signalling (mediated
114 by both AMPA and NMDA receptors) ^{2,32–39}. Ketamine (a dissociative anaesthetic at
115 high doses, and atypical psychedelic at low doses) is an NMDA receptor antagonist
116 ^{40–45}; the classic psychedelics LSD and DMT are agonists of the serotonin 2A
117 receptor, with a strong dependence between subjective efficacy and 2A receptor
118 affinity ^{46–49}.

119 However, in the words of Sleight and colleagues, “Linking observed molecular actions
120 for any particular drug with its clinical effects is an abiding pharmacological problem”
121 ⁵⁰: knowing the primary molecular target is not sufficient to understand a drug’s
122 effects on brain function, for several reasons. First, given the brain’s intricate, nested
123 feedback loops and recurrent pathways of connectivity, even a relatively selective
124 drug can end up influencing unrelated systems beyond what may be apparent from
125 in vitro studies. Second, most mind-altering compounds are also known to have
126 affinity for other receptors. Indeed, evidence has been accumulating that multiple
127 neurotransmitter influences may be involved in both the neural and subjective
128 experiences induced by many consciousness-altering drugs. In the last year, human
129 neuroimaging studies identified the involvement of the dopaminergic system in both
130 propofol-induced anaesthesia ⁵¹ and the subjective effects of LSD ⁵². More broadly, a
131 recent large-scale study, combining receptor expression from transcriptomic data
132 with linguistic processing of several thousand subjective reports of psychedelic use,
133 identified complex multivariate patterns of association between neurotransmitters
134 and their effects on the mind elicited by a wide variety of psychedelics, even for
135 putatively selective agents ⁵³. At the same time, molecularly different compounds can
136 exert intriguingly similar effects on both the mind and brain: for instance, LSD and
137 (sub-anaesthetic) ketamine can produce subjectively similar effects and changes in
138 terms of structure-function coupling and the complexity of brain activity - despite
139 acting on different pathways ²¹. This suggests both divergent and convergent effects
140 of different pharmacological agents on the brain’s rich neurotransmitter landscape.

141 Finally, the human brain exhibits rich patterns of anatomical, functional,
142 cytoarchitectonic, and molecular variations ^{54–59}. Such patterns also extend to the
143 regional distribution of different neurotransmitter receptors and transporters, which
144 vary widely not only in terms of their affinity, time-scales, and downstream effects on

145 neuronal excitability, but also their distribution across regions, layers and neuron
146 types ^{27–30}. Therefore, our knowledge of how a drug influences neurotransmission
147 must take into account the neuroanatomical distribution of its target
148 neurotransmitters - an essential step towards explaining how different
149 neurotransmitters mediate the capacity of different drugs to shape the functional and
150 computational properties of the brain's architecture ^{27,31}.

151 Here, we sought to address this question in a data-driven way, mapping the
152 neurotransmitter landscape of drug-induced alterations in the brain's functional
153 connectivity. To do so, we leveraged two unique datasets: (i) a recently assembled
154 collection of in vivo maps of regional receptor expression from 18 different receptors,
155 obtained from PET scanning of over 1200 total subjects, providing the most detailed
156 information about neuromodulators and their spatial distribution available to date ³¹;
157 and (ii) resting-state functional MRI (rs-fMRI) data acquired under the effects of the
158 classic psychedelics LSD ⁶⁰ and ayahuasca ⁶²; the atypical psychedelic ketamine (at
159 sub-anaesthetic dose) ⁶³; the cognitive enhancers modafinil ⁶⁴ and methylphenidate
160 ¹⁰; and the anaesthetics sevoflurane ⁶⁵ and propofol ^{66,67} (which we compared
161 against pre-anaesthetic baseline as well as post-anaesthetic recovery); representing
162 a total of 272 sessions of pharmacological-MRI from 114 distinct subjects and 7
163 distinct pharmacological agents. Through pharmacologically modulated rs-fMRI, we
164 can characterise a drug's effects on the brain's spontaneous activity, without the
165 interference of any specific task ¹.

166 Thus, our goal was to obtain a comprehensive mapping between the cortical
167 distributions of neurotransmitters and a set of diverse psychoactive pharmacological
168 agents (covering the range from anaesthetics to psychedelics), in terms of their
169 effects of functional connectivity. There have been other studies looking at the
170 relationships between brain changes induced by one or few psychoactive drugs, and
171 one or few neurotransmitter systems ^{51,52,68–73}. However, to our knowledge, this is the
172 largest fMRI study both in terms of the number and variety of psychoactive
173 pharmacological agents, and the breadth of neurotransmitter systems considered.

174

175 Results

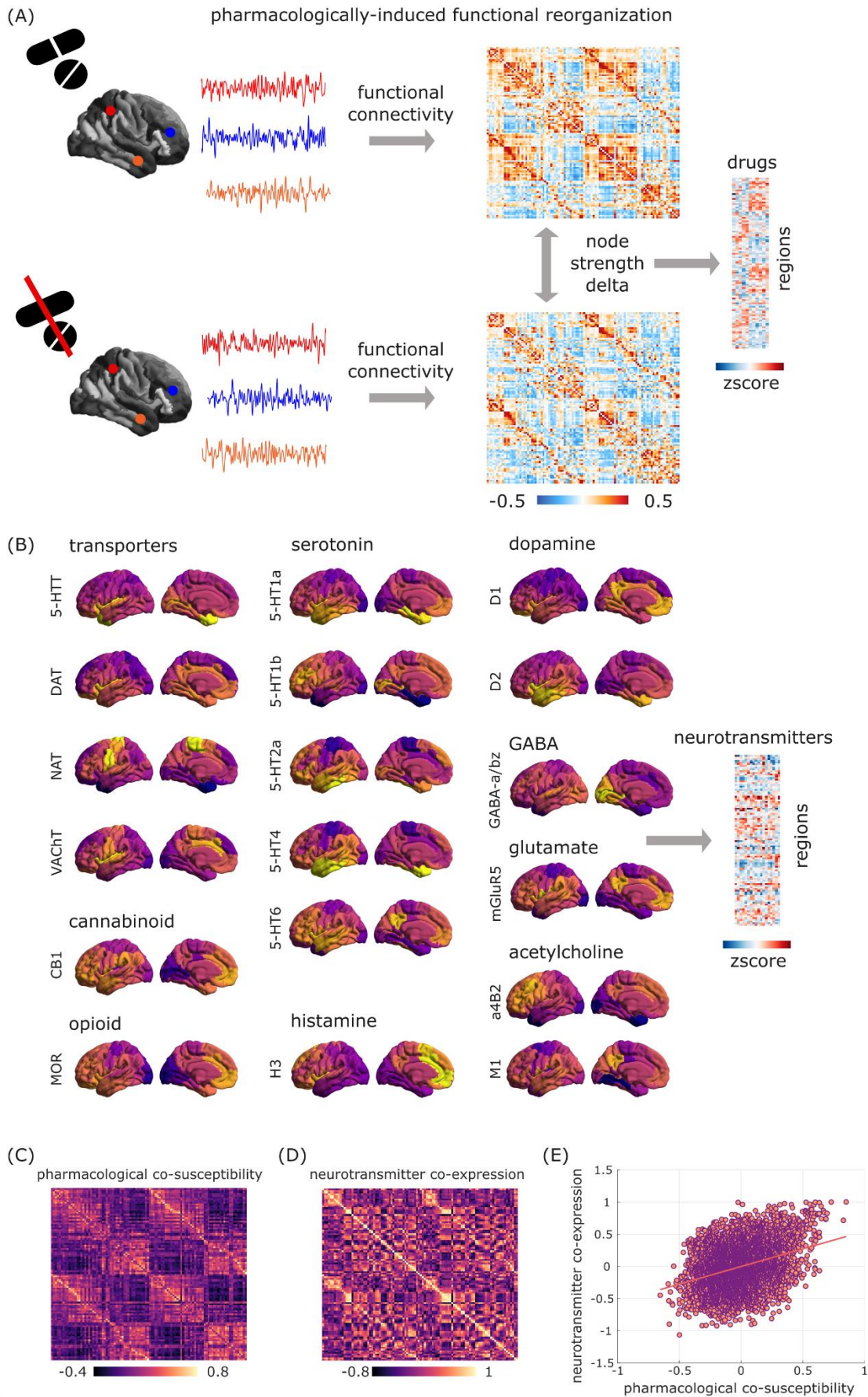
176

177 To establish a relationship between neurotransmitter systems and
178 pharmacologically-induced reorganisation of the brain's functional architecture, we
179 combine two sets of neuroimaging data, each collected from across multiple studies.
180 On one hand, we characterise drug-induced functional reorganisation as the
181 changes in functional connectivity (FC) obtained by contrasting resting-state
182 functional MRI (rs-fMRI) at baseline and under the acute effect of a psychoactive
183 drug. We considered the general anaesthetics propofol (two independent datasets)
184 and sevoflurane; the cognitive enhancers modafinil and methylphenidate; the
185 "atypical" psychedelic ketamine (at sub-anaesthetic doses); and the classic
186 psychedelics ayahuasca and lysergic acid diethylamide (LSD) (Figure 1). For each
187 anaesthetic, we considered two contrasts: drug versus pre-induction baseline, and
188 drug versus post-anaesthetic recovery.

189

190 On the other hand, we consider the cortical distribution of 14 neurotransmitter
191 receptors and 4 transporters, obtained from in vivo Positron Emission Tomography
192 ³¹. Overall, 9 neurotransmitter and neuromodulatory systems ("neurotransmitters" for
193 short) are covered: dopamine (D1 ⁷⁴, D2 ⁷⁵⁻⁷⁸, DAT ⁷⁹), norepinephrine (NET ⁸⁰⁻⁸³),
194 serotonin (5-HT1A ⁸⁴, 5-HT1B ^{84-87,87-89}, 5-HT2A ⁹⁰, 5-HT4 ⁹⁰, 5-HT6 ^{91,92}, 5-HTT ⁹⁰),
195 acetylcholine ($\alpha4\beta2$ ^{93,94}, M1 ⁹⁵, VAcHT ^{96,97}), glutamate (mGluR5 ^{98,99}), GABA
196 (GABA-A ¹⁰⁰), histamine (H3 ¹⁰¹), cannabinoid (CB1 ¹⁰²⁻¹⁰⁵), and opioid (MOR ¹⁰⁶).
197 (Figure 1). Both rs-fMRI and PET maps were parcellated into 100 functionally
198 defined regions according to the Schaefer atlas ¹⁰⁷; results for the subcortex and for
199 a different cortical parcellation (Lausanne-114 ¹⁰⁸) are provided as Supplementary
200 Information.

201



203 **Figure 1. Overview of receptors and pharmacological rs-fMRI data.** (A) For each psychoactive
204 drug, its pattern of pharmacologically-induced functional reorganisation is quantified as the average
205 (across subjects) of the within-subject difference in regional FC density between task-free fMRI scans
206 at baseline and under the drug's effects. The result is a map of 100 cortical regions by 11 drug-related
207 contrasts. (B) Neurotransmitter systems are mapped with Positron Emission Tomography with
208 radioligands for 14 receptors and 4 transporters, resulting in a map of 100 cortical regions by 18
209 neurotransmitters. Correlating each of these sets of maps against itself yields two region-by-region
210 matrices of pharmacological co-susceptibility (C) and neurotransmitter co-expression (D),
211 respectively, which are significantly correlated even after removing the exponential relationship with
212 Euclidean distance between regions (E).

213

214 Brain regions with shared chemoarchitecture also respond 215 similarly across pharmacological perturbations

216

217 Receptors and transporters shape the way that neurons respond to
218 neurotransmission and neuromodulatory influences. In turn, psychoactive drugs
219 exert their effects (primarily) by acting on neurotransmitters and neuromodulators.
220 Therefore, we reasoned that everything else being equal, regions that express
221 similar patterns of receptors and transporters should exhibit similar patterns of
222 susceptibility to drug-induced functional reorganisation.

223

224 To address this question, we computed matrices of pharmacological co-susceptibility
225 and neurotransmitter co-expression between pairs of regions, by correlating
226 respectively the regional patterns of drug-induced FC changes (across all subjects),
227 and the regional patterns of neurotransmitter expression across all 18 receptor and
228 transporter PET maps. To account for spatial autocorrelation in molecular and FC
229 attributes, we regressed out from both matrices the exponential trend with Euclidean
230 distance^{109–112}.

231

232 Supporting our hypothesis, we found that pharmacological co-susceptibility is
233 significantly correlated with neurotransmitter profile similarity: the extent to which two
234 regions' FC patterns are similarly affected by perturbations induced by different
235 psychoactive drugs, is predicted by the extent to which they co-express
236 neurotransmitter receptors and transporters: $\rho = 0.26$, $p < 0.001$ after regressing
237 out the effects of Euclidean distance (Figure 1). In other words, regions that exhibit
238 shared chemoarchitecture also respond similarly across pharmacological
239 perturbations.

240

241 Multivariate Receptor-Drug Associations

242

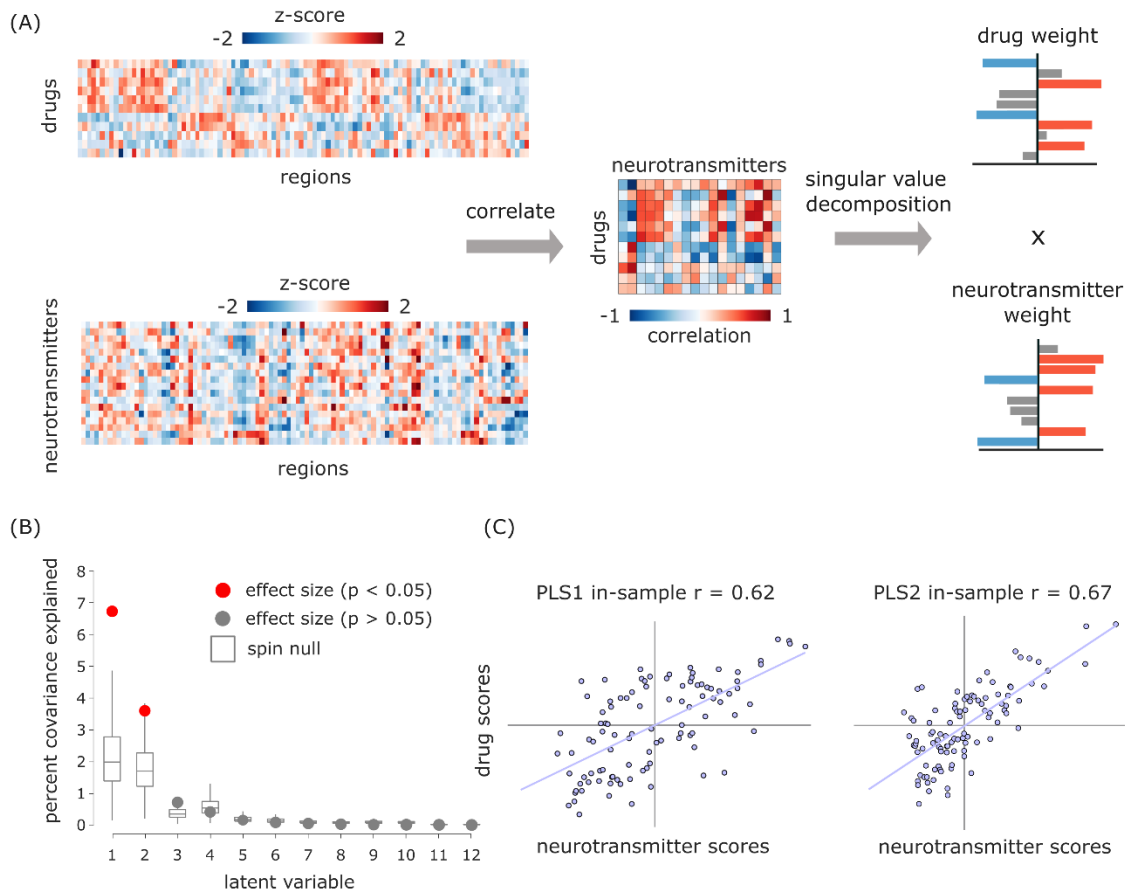
243 The previous analysis revealed of a relationship between large-scale patterns of
244 neurotransmitter expression and large-scale patterns of functional susceptibility to
245 pharmacological perturbations - complementing previous work that identified
246 relationships between individual drugs and individual receptors. However, neither of
247 these two approaches captures the full richness of the two datasets employed here.
248 To obtain a synthesis between these two approaches, we employed a multivariate
249 association technique, Partial Least Squares correlation (PLS, also known as
250 Projection to Latent Structures ^{113,114}), which enabled us to identify multivariate
251 patterns of maximum covariance between drug-induced effects on functional
252 connectivity, and the cortical distributions of neurotransmitter expression ^{115,116}.

253

254 This analysis indicated the presence of two statistically significant latent variables
255 (linear weighted combinations of the original variables) relating pharmacologically-
256 induced functional reorganisation to neurotransmitter profiles. Significance was
257 assessed against autocorrelation-preserving spin-based null models, embodying the
258 null hypothesis that drug effects and neurotransmitters are spatially correlated with
259 each other purely because of inherent spatial autocorrelation ¹¹⁷⁻¹²⁰ (Figure 2). We
260 further cross-validated this result using a distance-dependent method; out-of-sample
261 $r = 0.40$ for PLS1 and 0.59 for PLS2, both $p < 0.001$ from t-test against spin-based
262 null distributions) (Figure S1).

263

264



265

266 **Figure 2. PLS analysis reveals spatially covarying patterns of pharmacologically-induced**
267 **functional reorganisation and neurotransmitter expression.** (A) PLS analysis relates two data
268 domains by correlating the variables across brain regions and subjecting this to singular value
269 decomposition. This results in multiple latent variables: linear weighted combinations of the original
270 variables (neurotransmitter weights and drug weights) that maximally covary with each other. (B)
271 Latent variables are ordered according to effect size (the proportion of covariance explained between
272 neurotransmitter expression and drug-induced functional reorganisation they account for) and shown
273 as red dots. (C) The first two latent variables (PLS1 and PLS2) were statistically significant, with
274 respect to the spatial autocorrelation-preserving null model shown in grey (10,000 repetitions).
275 Neurotransmitter (drug) scores are defined as the projection of the original neurotransmitter density
276 (drug-induced FC changes) matrix onto the neurotransmitter (drug) weights, such that each brain
277 region is associated with a neurotransmitter and drug score. By design, neurotransmitter and drug
278 scores correlate highly.

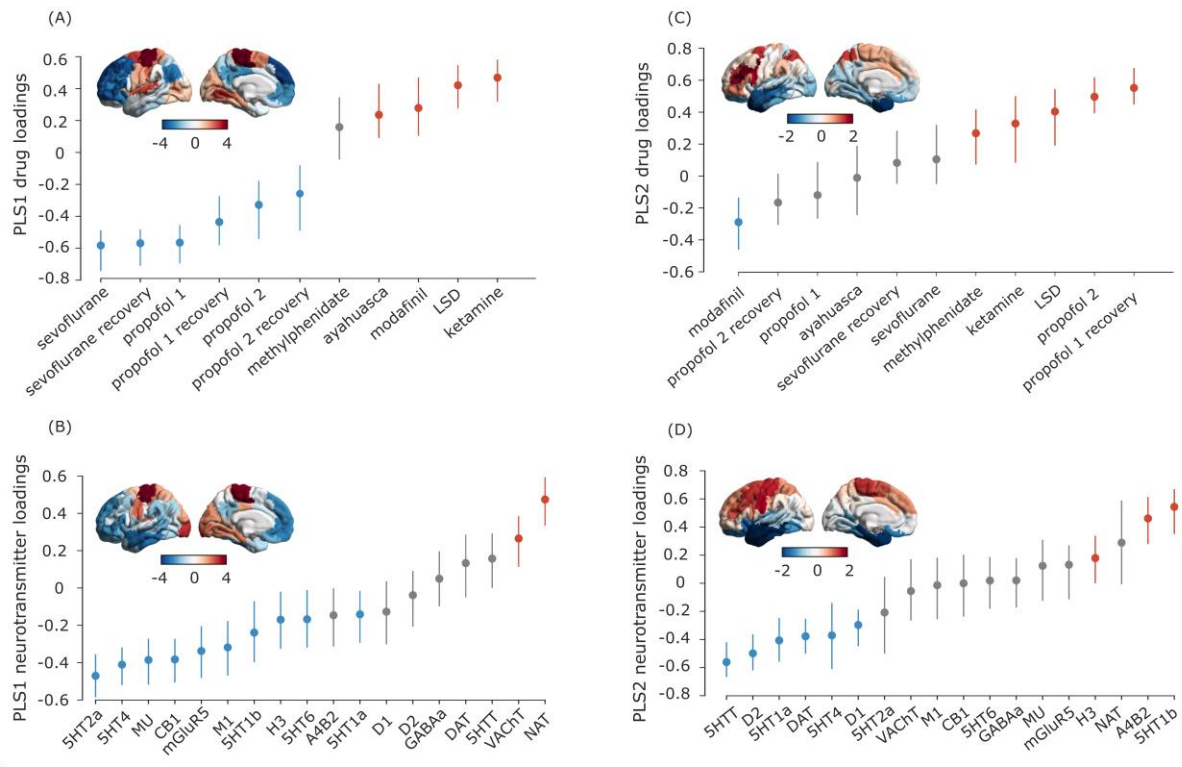
279

280

281 For each latent variable, each brain region is associated with a neurotransmitter and
282 drug score. In turn, neurotransmitter (drug) loadings are defined as the correlation
283 between the PLS-derived score pattern and each neurotransmitter's density of
284 expression (resp., drug-induced FC changes) across brain regions. Taking into
285 account the first latent variable (PLS1), drug loadings showed a distinction of
286 pharmacological effects into two groups, with anaesthetics on one end, and

287 psychedelics and cognitive enhancers on the other. Neurotransmitter loadings
288 divided the receptors from transporters: at the positive end (orange), the
289 acetylcholine and noradrenaline transporters (with the serotonin and dopamine
290 transporters immediately following, but including zero in their 95% CI); all receptors
291 were instead at the negative end (blue), although some included zero in their CI
292 (Figure 3).

293



294

295 **Figure 3. PLS scores and loadings from significant latent variables.** (A-B) Scores and loadings
296 for PLS1. (C-D) scores and loadings for PLS2. Brain plots: Drug scores (top row) and
297 neurotransmitter scores (bottom row) for each brain region are obtained by projecting the original
298 neurotransmitter and drug data back onto the PLS analysis-defined drug/neurotransmitter weights,
299 indexing the extent to which a brain region expresses covarying drug/ neurotransmitter patterns. In
300 turn, neurotransmitter (drug) loadings are defined as the Pearson's correlation between each
301 neurotransmitter's density of expression (drug-induced FC changes) across brain regions and the
302 PLS analysis-derived score pattern. Error bars indicate 95% confidence interval, and colour indicates
303 direction of the effect: positive (orange), negative (blue), or null (grey). Same-coloured loadings and
304 scores co-vary positively, whereas opposite-coloured drugs and scores co-vary negatively.

305

306

307 Pertaining to the second latent variable (PLS2), neurotransmitter loadings largely set
308 apart the monoamines dopamine and serotonin (except 5HT-1b) on one end, from
309 the other neurotransmitters on the other end. However, the drug loadings were less

310 clearly discernible, with propofol at both ends. Both neurotransmitter and drug scores
311 markedly separated dorsal and ventral aspects of the brain for this second latent
312 variable (Figure 3).

313

314 Pharmacologically-induced alterations align with functional, 315 anatomical and molecular hierarchies

316

317 Neurotransmitter and drug scores (whose spatial similarity PLS is designed to
318 maximise) provide information about the regional distribution of neurotransmitter-
319 drug associations. Neurotransmitters and drugs whose activity correlates positively
320 with the score pattern covary with one another in the positively scored regions, and
321 vice versa for negatively scored regions.

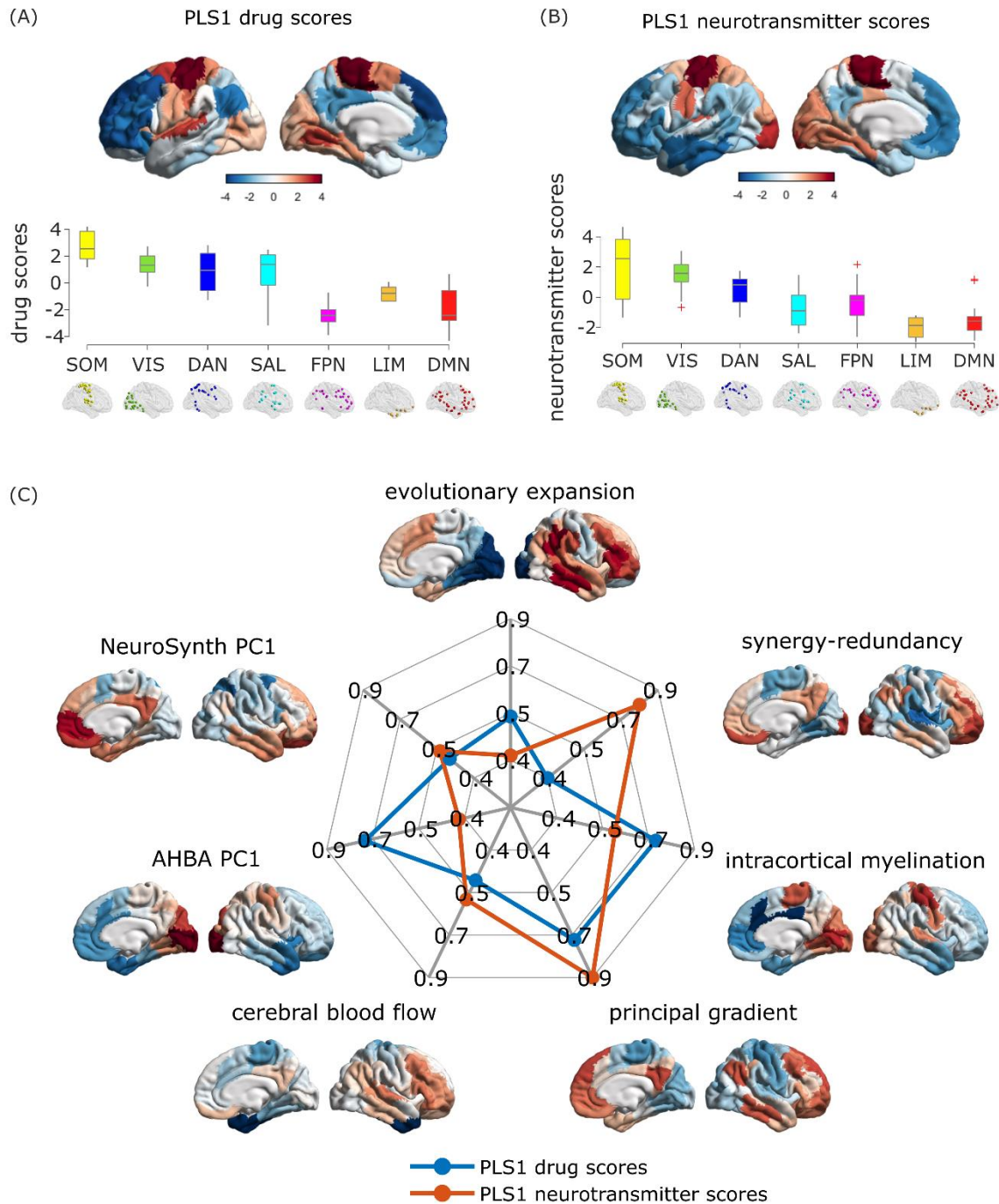
322

323 PLS1 scores correspond to the main axis of covariance between neurotransmitter
324 expression and pharmacologically-induced functional reorganisation. For both drug
325 and receptor scores, we observed that their regional distribution reflected the brain's
326 organisation into intrinsic resting-state networks (RSNs) ¹²¹, setting apart visual and
327 somatomotor cortices from association cortices (Figure 3,4). It is possible that the
328 correspondence of PLS1 scores with RSNs may be in part driven by the fact that
329 these networks are predicated in terms of functional neuroimaging, which we also
330 used to characterise drug-induced functional reorganisation in our data. Therefore,
331 we next sought to determine whether our data-driven topographic patterns reflect
332 other cortical gradients of variation in terms of functional, anatomical, and molecular
333 attributes. To this end, we considered intracortical myelination obtained from
334 T1w/T2w MRI ratio ⁵⁸; evolutionary cortical expansion obtained by comparing human
335 and macaque ¹²²; the principal component of variation in gene expression from the
336 Allen Human Brain Atlas transcriptomic database ("AHBA PC1") ^{59,123}; the principal
337 component of variation in task activation from the NeuroSynth database
338 ("NeuroSynth PC1") ^{59,124}; and the principal gradient of functional connectivity ⁵⁷.
339 Since pharmacological interventions exert their effects on the brain via the
340 bloodstream, we also included a map of cerebral blood flow ⁵⁴. Finally, we included a
341 recently derived gradient of regional prevalence of different kinds of information, from
342 redundancy to synergy ¹²⁵.

343

344 We observed significant correlations (assessed against spin-based null models)
345 between each cortical hierarchy and both neurotransmitter and drug scores for PLS1
346 (note that the myelin and AHBA PC1 maps are reversed with respect to the
347 remaining hierarchies) (Figure 4). We also repeated this analysis for each of the
348 individual patterns of pharmacologically-induced functional reorganisation (Figure
349 S2). Even after FDR correction for multiple comparisons, each hierarchical gradient
350 was correlated with multiple patterns of pharmacologically-induced reorganisation,
351 and each drug (except methylphenidate) was correlated with multiple hierarchical
352 gradients. Once again, all anaesthetics exhibited similar patterns, opposite to the
353 pattern of correlations displayed by modafinil and the psychedelics ketamine, LSD
354 and ayahuasca. The only exception was methylphenidate, which exhibited no
355 significant correlations (Figure S2).

356



357

358 **Figure 4. Correspondence between the principal axis of drug-neurotransmitter scores and**
 359 **functional, anatomical and molecular hierarchies.** (A-B) Cortical distribution of drug and
 360 neurotransmitter scores for PLS1, and their association with intrinsic resting-state networks. (C)
 361 Radial plot represents the absolute value of the correlation between PLS1 drug and neurotransmitter
 362 scores, and each of seven cortical hierarchies obtained from different neuroimaging modalities. The
 363 magnitude of each correlation was statistically significant, as assessed against spin-based null
 364 models with preserved spatial autocorrelation.

365

366

367 The scores for PLS2 instead identified a ventral-dorsal pattern of regional variation
368 (Figure 3 and Figure S3), which did not significantly correlate with any of the
369 canonical gradients of hierarchical organisation (all $p > 0.05$ against spin-based null
370 models).

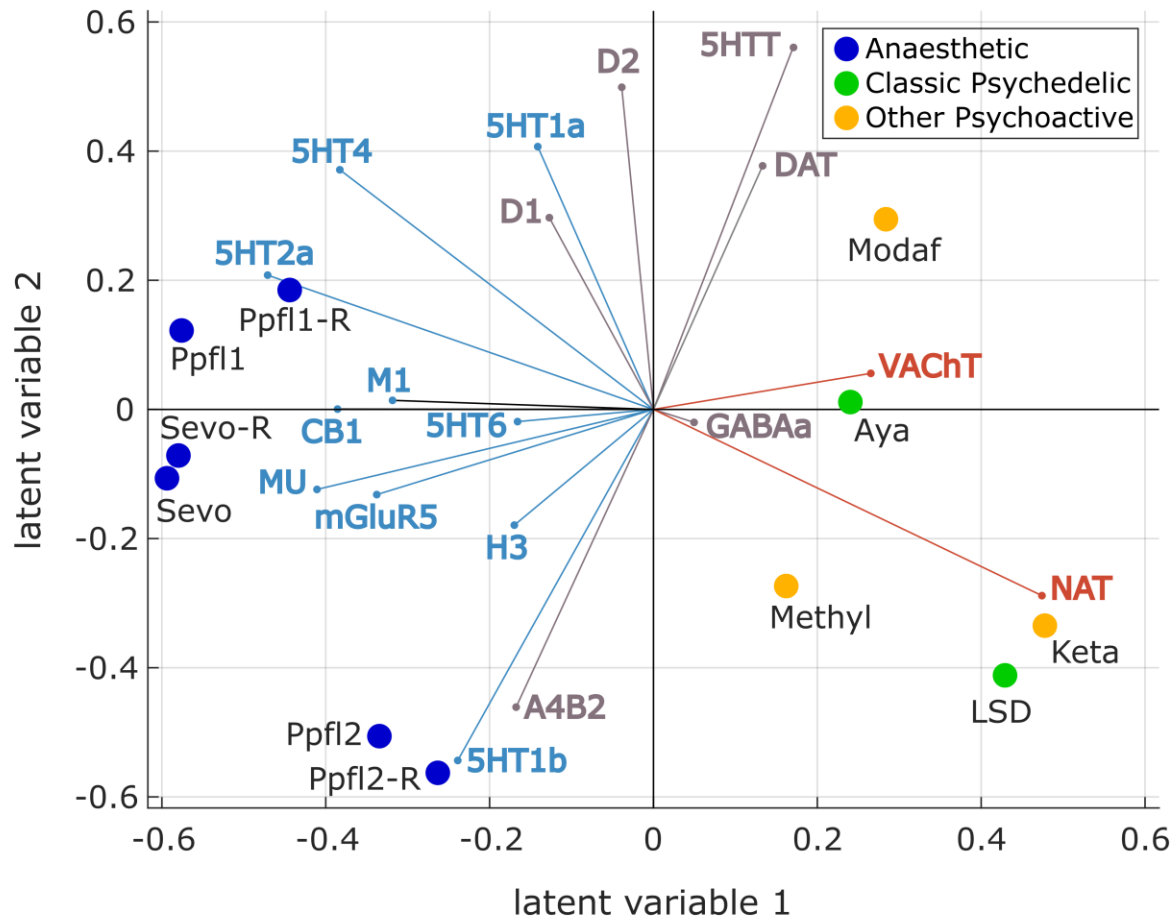
371

372 Neurotransmitter landscape of pharmacologically-induced 373 functional reorganisation

374

375 Taking into account the first two PLS latent variables shows how each drug-specific
376 pattern of pharmacologically-induced functional reorganisation can be interpreted in
377 terms of contributions from different receptors (note that sign is arbitrary) (Figure 5).
378 As already shown in Figure 3, the first latent variable revealed a stark division
379 between transporters and receptors, which discriminates between anaesthetics and
380 other psychoactive substances. In terms of pharmacological alterations, the non-
381 monoaminergic end of the second latent variable loaded onto drugs with relatively
382 stronger effects on subjective experiences (the higher doses of anaesthetic, and the
383 hallucinogenic psychedelics). However, methylphenidate also loaded onto this end of
384 the second latent variable. Altogether, we find that the first latent variable captures a
385 strong relationship between drug interventions and receptor systems that is both
386 biologically relevant and aligns with the functional organisation of the brain.

387



388

389 **Figure 5. Biplot of neurotransmitters and pharmacological agents.** Each drug is represented as a
390 point reflecting its projection onto the first two latent variables of the PLS analysis, color-coded based
391 on its effects on subjective experience (anaesthetic, psychedelic, or cognitive enhancer). Each
392 neurotransmitter receptor and transporter is represented as a vector in the same 2D space, color-
393 coded by loading onto PLS1 as shown in Figure 3 (orange for positive; blue for negative; and grey if
394 the 95% CI intersects zero).

395

396 Co-susceptibility to pharmacological and pathological 397 alterations

398 Finally, we wondered if the functional co-susceptibility of different regions to transient
399 pharmacological perturbations may provide a functional proxy for their co-
400 susceptibility to structural perturbations resulting from different neurological,
401 neurodevelopmental, and psychiatric disorders. To this end, we combined 11 spatial
402 maps of cortical thickness abnormalities made available by the Enhancing Neuro
403 Imaging Genetics Through Meta Analysis (ENIGMA) consortium ¹²⁶: 22q11.2
404 deletion syndrome (22q) ¹²⁷, attention-deficit/hyperactivity disorder (ADHD) ¹²⁸,
405 autism spectrum disorder (ASD) ¹²⁹, idiopathic generalized epilepsy ¹³⁰, right

406 temporal lobe epilepsy ¹³⁰, left temporal lobe epilepsy ¹³⁰, depression ¹³¹, obsessive-
407 compulsive disorder (OCD) ¹³², schizophrenia ¹³³, bipolar disorder (BD) ¹³⁴, and
408 Parkinson's disease (PD) ¹³⁵. For simplicity, we refer to diseases, disorders, and
409 conditions as "disorders" throughout the text. The cortical abnormality maps
410 summarise contrasts between over 21,000 adult patients and 26,000 controls,
411 collected following identical processing protocols to ensure maximal comparability
412 ¹²⁶.

413

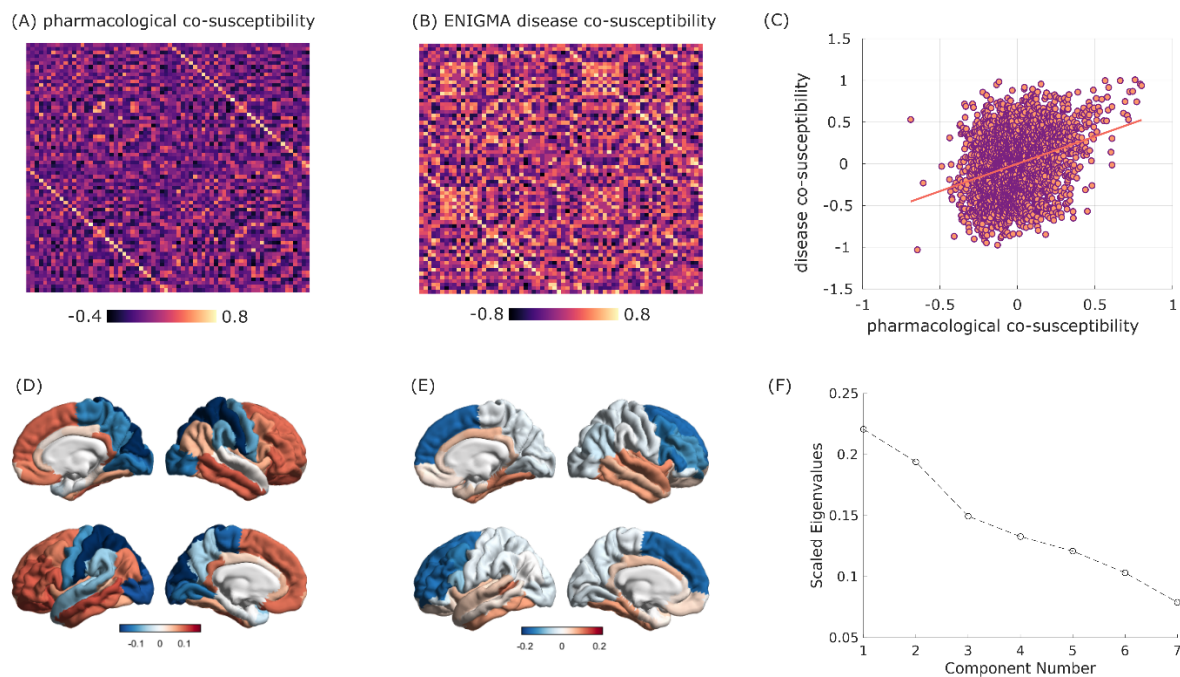
414 Following the same procedure used to obtain the region x region matrices of
415 pharmacological co-susceptibility and neurotransmitter co-expression in Figure 1, we
416 obtained a region x region matrix of co-susceptibility to disorder-induced cortical
417 abnormality by correlating the regional patterns of cortical abnormality across all 11
418 disorders ¹⁰⁹ (Figure 6A,B). Correlating this matrix of regional co-susceptibility to
419 disease-associated perturbations against the previously derived matrix of regional
420 co-susceptibility to pharmacological perturbations, we found a statistically significant
421 relationship (Spearman's $\rho = 0.29$, $p < 0.001$ after regressing out the effect of
422 Euclidean distance) (Figure 6C). This result goes beyond a recent demonstration
423 that molecular similarity and disorder similarity are correlated ¹⁰⁹, by showing that a
424 correlation also exists between different kinds of perturbations: anatomical and
425 pharmacological.

426

427 This observation suggests that there may be common patterns of regional co-
428 susceptibility to perturbations, whether structural or functional. To explore this
429 possibility explicitly, we resorted to a non-linear dimensionality reduction algorithm,
430 diffusion map embedding, to obtain joint gradients of variation from pharmacological
431 and disease-associated co-susceptibility using a recently developed method for
432 network fusion ¹³⁶. We found that the main axis of variation in regional joint
433 susceptibility to pharmacological and neuropsychiatric alterations corresponds to the
434 well-known principal gradient of functional connectivity ⁵⁷, setting apart unimodal
435 from transmodal cortices, reminiscent of the PLS1 scores (Figure 6D). The second
436 gradient instead sets apart dorsal and ventral parts of the brain, reminiscent of the
437 PLS2 scores (Figure 6E). Together, these two gradients account for nearly half of
438 the variation in regional co-susceptibility (Figure 6F).

439

440 When applying diffusion map embedding to the matrix of pharmacological co-
441 susceptibility only, we found that the first two gradients of variation in regional
442 pharmacological susceptibility coincide with the two principal gradients of functional
443 connectivity of Margulies et al ⁵⁷ (Figure S4): the first gradient sets apart unimodal
444 from transmodal cortices, coinciding with the first gradient of joint susceptibility,
445 whereas the second gradient is anchored in visual cortex at one end, and
446 somatomotor cortex at the other end (Figure S4). This observation suggests that co-
447 susceptibility to pharmacological perturbations recapitulates intrinsic functional
448 architecture, as well as the co-susceptibility to disorder-induced structural
449 perturbations.



450 **Figure 6. Co-susceptibility to pharmacological and pathological alterations.** Brain regions that
451 are similarly affected by pharmacology, in terms of functional reorganisation (A) are also similarly
452 affected across disorders (B), in terms of cortical thickness abnormalities. This relationship persists
453 after regressing out the exponential trend with Euclidean distance (C). (D-E) First two principal
454 gradients of regional joint susceptibility to pharmacological and neuropsychiatric and neurological
455 alterations. (F) Scree plot of the scaled eigenvalues from diffusion map embedding versus number of
456 components.
457

458
459

460 Discussion

461

462 Here, we characterised how mind-altering pharmacological agents engage the
463 brain's rich neurotransmitter landscape to exert their effects on brain function. We
464 mapped the functional chemoarchitecture of the human brain, by developing a
465 computational framework to relate the regional reorganisation of fMRI functional
466 connectivity induced by 8 different mind-altering drugs, and the cortical distribution of
467 18 neurotransmitter receptors and transporters obtained from PET ³¹. This approach
468 allowed us to discover large-scale spatial gradients relating pharmacologically-
469 induced changes in functional connectivity to the underlying neurotransmitter
470 systems. By relating microscale molecular chemoarchitecture and macroscale
471 functional reorganisation induced by drugs with potent acute effects on the mind, our
472 results provide a first step to bridge molecular mechanisms and their effects on
473 subjective experience, cognition, and behaviour, via their effects on the brain's
474 functional architecture.

475

476 Using our computational framework, we found that psychoactive drugs are best
477 understood in terms of contributions from multiple neurotransmitter systems. We also
478 found that anaesthetics and psychedelics/cognitive enhancers are largely opposite in
479 terms of their association with neurotransmitters in the cortex. Remarkably, the
480 effects of both anaesthetics and psychedelics/cognitive enhancers on brain function,
481 though opposite, are both topographically organised along multiple hierarchical
482 gradients of brain function, anatomy, and neurobiology. Finally, we found that co-
483 susceptibility to pharmacological perturbations recapitulates co-susceptibility to
484 disorder-induced structural perturbations.

485

486 Many of the drugs considered here are known to have varied molecular targets,
487 beyond the primary ones through which they exert their effects. The present results
488 add another dimension to recent work employing a similar multivariate approach to
489 relate gene expression of receptors with subjective reports of psychedelic
490 experiences, which also found widespread involvement of multiple receptors ⁵³. In
491 addition, all the drugs we considered here have profound effects on the mind after a
492 single acute dose, from cognitive enhancement to hallucinations to the suppression

493 of consciousness altogether. Such far-reaching effects are accompanied by
494 sometimes drastic repercussions on brain function and dynamics: it stands to reason
495 that such widespread reorganisation would not leave many neurotransmitter
496 pathways unaffected - even those that are not directly involved in generating the
497 altered state in question.

498

499 The opposite characterisation of psychedelics and anaesthetics is aligned with their
500 respective effects on the complexity of brain activity and connectivity, which is
501 reduced by anaesthesia but increased by LSD, ayahuasca and ketamine, as well as
502 other psychedelics ^{18,21,23,62,137–147}. Similarly, psychedelics (including sub-anaesthetic
503 ketamine) and anaesthetics were recently shown to exert opposite effects on
504 structure-function coupling: whereas anaesthesia increases the dependence of brain
505 activity on the underlying structural network, LSD, psilocybin, and sub-anaesthetic
506 ketamine induce fMRI BOLD signals that are increasingly liberal with respect to the
507 underlying structural network organisation ²¹.

508

509 The main division we observed in terms of neurotransmitters is between receptors
510 and transporters, which displayed opposite associations with drug-induced effects.
511 Specifically pertaining to PLS1, we found that transporters covary with cognitive
512 enhancers and psychedelics in primary sensory and motor regions, whereas
513 receptors covary with anaesthetics in transmodal association cortices. Hierarchical
514 organisation of pharmacologically-induced functional reorganisation stands to reason
515 based on prior evidence: both psychedelics and GABA-ergic anaesthetics have been
516 shown to have potent effects on the activity and connectivity of higher-order
517 association cortices, and the default mode network in particular ^{18,60,61,65,148–151}. In
518 addition, serotonergic psychedelics also exert powerful influences on the visual
519 cortex at the other end of the cortical hierarchy ⁶⁰, and as a result they have been
520 shown to induce a “flattening” of the principal gradient of functional connectivity ¹⁵².

521

522 Having established that the effects of mind-altering drugs are hierarchically
523 organised, the question then becomes: why should mind-altering drugs exert their
524 effects in such a hierarchically organised fashion? Multiple aspects of neuroanatomy
525 may contribute to this effect. First, the principal component of variation of receptor
526 expression is itself organised along the brain’s sensory-to-association hierarchical

527 axis ²⁷ - and so is, for instance, the distribution of the serotonin 2A receptor, the main
528 direct target of serotonergic psychedelics ³¹. Second, transmodal cortices are
529 characterised by increased excitability ¹⁵³ and a predominance of feedback efferent
530 connections ²⁷: combined with their high diversity of receptor expression across
531 layers ²⁷, these regions may be especially susceptible to receive and amplify multiple
532 pharmacological influences.

533

534 Third, we observed that for most drugs, pharmacologically-induced changes in
535 functional connectivity correlate with the map of regional cerebral blood flow; since
536 ultimately the bloodstream is how drugs reach their regional molecular targets,
537 greater cerebral blood flow in transmodal cortices may facilitate especially high
538 availability of the drug in these regions (although it should be noted that some drugs
539 can also have effects on heart rate and neuro-vascular coupling). Finally, regions of
540 transmodal cortex have high neuron density ¹⁵⁴ and tend to have numerous, far-
541 reaching, and diversely distributed anatomical connections with the rest of the brain
542 ¹⁵⁵, so that any effects that are exerted there may quickly reverberate throughout the
543 whole cortex.

544

545 To summarise, we conjecture that the hierarchical organisation of pharmacologically-
546 induced changes in FC may be explained as follows: transmodal association cortices
547 are especially diverse in their receptor profiles, and rich in some key receptors; in
548 addition to being more susceptible to pharmacological intervention due to higher
549 expression of receptors, blood flow is poised to bring greater amounts of drug to
550 these very cortices; and once these cortices' activity is perturbed, the perturbation
551 can reverberate widely, thanks to their widespread connectivity. Of course, the drugs
552 we included were chosen precisely because of their powerful effects on cognition
553 and subjective experience, so it stands to reason that their effects should align with
554 the division between primary and higher-order cortices (which also aligns with the
555 principal component of variation obtained from NeuroSynth term-based meta-
556 analysis). In other words, drugs whose effects on functional connectivity are less
557 selective for higher versus lower ends of the cortical hierarchy may simply be less
558 likely to exert mind-altering effects of the kind that we chose to focus on in this work.

559

560 More broadly, we found that pairs of regions that are more similar in terms of their
561 susceptibility to pharmacologically-induced FC changes, are also more similar in
562 their susceptibility to cortical alterations associated with a variety of neuropsychiatric
563 disorders. This observation suggests a broader pattern of both (acute)
564 pharmacological and (chronic) neuroanatomical susceptibility across regions. We
565 found that this joint vulnerability can be understood in terms of two multimodal
566 principal gradients of variation over the cortex: one of them resembling the principal
567 gradient of functional connectivity (and principal latent variable of neurotransmitter-
568 drug association), and the other anchored in dorsal prefrontal cortex at one end, and
569 temporal cortex at the other. The association between disorder co-susceptibility and
570 co-susceptibility to pharmacologically-induced functional reorganisation sheds new
571 light on recent evidence that the principal gradient of neurotransmitter expression is
572 particularly relevant for predicting a wide spectrum of disease-specific cortical
573 morphology ¹⁰⁹, by showing that this observation extends to the effects of engaging
574 different receptors. This interpretation is further supported by our own evidence that
575 pharmacological perturbations are shaped by neurotransmitter co-expression.

576

577 The results reported here open new possibilities for data-driven, multivariate
578 mapping between the brain's high-dimensional neurotransmitter landscape and the
579 effects of potent pharmacological interventions on the brain's functional architecture.
580 Crucially, neuropsychiatric disorders and candidate pharmacological treatments for
581 them ultimately need to exert their effects on cognition and behaviour by influencing
582 brain function. In this light, it is intriguing that susceptibility to disorder-related cortical
583 abnormalities correlates with susceptibility to pharmacological intervention. This
584 observation suggests that regions that are structurally most vulnerable to disease
585 (which presumably in turn shapes their functional architecture) may also be the ones
586 that are most susceptible to re-balancing of their functional organisation by an
587 appropriate choice of pharmacological intervention. This work represents the
588 necessary first step towards identifying novel and perhaps unexpected associations
589 between drugs and neurotransmitters, as well as elucidating the known ones in a
590 data-driven manner.

591 Limitations and future directions

592 Although the main strength of our study is our extensive coverage of both
593 neurotransmitters and pharmacological data, it is important to acknowledge that
594 neither is complete: in particular, our sample did by no means exhaustively include
595 all mind-altering drugs that have been studied: prominent additions for future work
596 may include psilocybin, DMT (as separate from the other components of the
597 ayahuasca infusion)^{156,157}, the kappa opioid receptor agonist salvinorin-A¹⁵⁸, the
598 alpha-2 receptor agonist dexmedetomidine^{159–161}, and anaesthetic doses of
599 ketamine^{24,148,162}, just to name a few that have been recently studied - but also
600 alcohol or caffeine, arguably the two most widely used psychoactive substances.

601
602 We also acknowledge that the pharmacological datasets included here come from
603 limited samples that have been studied before, and replication in different datasets
604 with the same drugs (as we have done for propofol) would also be auspicious -
605 especially for the methylphenidate dataset, which unlike all our other data, comes
606 from TBI patients rather than healthy controls¹⁰. Although we have endeavoured to
607 mitigate scanner and acquisition differences by using a within-subject design and re-
608 preprocessing all data with the same pipeline, nevertheless we cannot exclude some
609 residual influence of such differences on our results (e.g., eyes open versus closed;
610 the ayahuasca data were acquired at a lower field strength of 1.5T; the sevoflurane
611 and modafinil data were acquired at higher temporal resolution, with TR = 1.83s and
612 1.671s, respectively). Similar considerations about the differences between datasets
613 apply for the PET data, as discussed in detail in the original publication collecting the
614 PET maps³¹. Likewise, the coverage of neurotransmitter receptors and transporters,
615 though the most extensive available to date, is far from exhaustive. The same
616 limitation also applies to the ENIGMA disorder data¹²⁶: many more disorders,
617 diseases, and conditions exist than the ones considered here. And although the
618 ENIGMA consortium provides datasets from large samples with standardised
619 pipelines, ensuring robust results, the patient populations may exhibit co-morbidities
620 and/or be undergoing treatment. In addition, the available maps do not directly reflect
621 changes in tissue volume, but rather the effect size of patient-control statistical
622 comparisons, in terms of only one low resolution cortical-only parcellation.

623

624 In addition to the inevitable limitations of analysing large-scale datasets from multiple
625 sites, there are also limitations of our analytic framework. Although we report a
626 macroscale spatial association between neurotransmitter expression and
627 pharmacologically-induced functional reorganisation that is statistically unexpected
628 based on autocorrelation alone, caution is warranted when drawing inferences from
629 statistical results to the underlying biology. We used linear models that assume
630 independence between observations - an assumption that mostly does not hold in
631 the brain, given the possibility of nonlinear effects in how drugs exert their effects on
632 the brain's intricately connected neurotransmitter systems. To mitigate this limitation,
633 throughout this work we triangulated towards a robust statistical mapping between
634 neurotransmitters and drugs by combining cross-validation and conservative null
635 models that account for the spatial dependencies between regions ⁵⁹.

636

637 Another limitation is that, due to data availability and well documented differences in
638 PET radioligand uptake between cortical and subcortical structures ^{31,163,164}, our work
639 was mainly restricted to the cortex. The thalamus, brainstem, and other subcortical
640 structures are prominently involved in mediating cortico-cortical interactions and the
641 effects of both psychedelics, anaesthetics, and cognitive enhancers ^{16,18,51,65,159,165–}
642 ¹⁷⁰. Although we did perform a separate PLS analysis on the subcortex (Fig. S6), we
643 expect that future work combining these approaches through suitable data (and
644 including cerebellum and brainstem) will provide richer insights than the sum of their
645 individual contributions.

646

647 More broadly, the other main limitation of this work is its correlational nature:
648 receptors and drugs were mapped in separate cohorts of individuals, and identifying
649 spatially correlated patterns does not guarantee the causal involvement of the
650 neurotransmitters in question. Experimental interventions will be required to
651 conclusively demonstrate causal involvement, and elucidate the underlying
652 neurobiological pathways. However, we emphasise that our results generate
653 empirically testable hypotheses about which neurotransmitters may be involved with
654 the macroscale effects of different drugs on brain function. Such hypotheses may be
655 tested experimentally, but also *in silico*: whole-brain computational modelling is
656 becoming increasingly prominent as a tool to investigate the causal mechanisms that
657 drive brain activity and organisation in healthy and pathological conditions ^{171–174}.

658 Crucially, the more biologically-inspired models (e.g. dynamic mean-field) can also
659 be enriched with further information, such as regional myelination ¹⁵³, or the regional
660 distribution of specific receptors and ion channels obtained from PET or
661 transcriptomics ^{70–72,175,176}, to reflect neurotransmitter influences. This approach may
662 complement experimental manipulations, making it possible to systematically
663 evaluate the causal effects of combinations of different neuromodulators on the
664 brain's functional connectivity.

665 Conclusion

666 Here, we mapped the functional chemoarchitecture of the human brain, by relating
667 the regional changes in fMRI functional connectivity induced by 7 different mind-
668 altering drugs, and the regional distribution of 18 neurotransmitter receptors and
669 transporters obtained from PET. This work provides a computational framework to
670 characterise how mind-altering pharmacological agents engage the brain's rich
671 neurotransmitter landscape to exert their effects on brain function. This analytic
672 workflow could find fruitful application for data-driven prediction of the brain effects of
673 candidate drugs: the mapping between neurotransmitters and pharmacological
674 effects on brain function offers an indispensable biological lens that can reveal
675 neurotransmitter targets for therapeutic intervention. In summary, we demonstrate
676 that manifold patterns of neurotransmitter expression are variously engaged by an
677 array of potent pharmacological interventions, ultimately manifesting as a large-scale
678 hierarchical axis. Collectively, these results highlight a statistical link between
679 molecular dynamics and drug-induced reorganisation of functional architecture.

680

681 Materials and Methods

682

683 Description of datasets

684

685 Propofol

686 Propofol (2,6-diisopropylphenol) is perhaps the most common agent used for
687 intravenous induction and maintenance of general anaesthesia ³². One of the chief
688 reasons for its widespread use, both in the operating room and for scientific studies,
689 is propofol's rapid action, which allow for precise titration and therefore greater
690 control over the induction and emergence process. Additionally, propofol has
691 minimal effects on both regional cerebral blood flow ¹⁷⁸, and the coupling between
692 blood flow and metabolism ¹⁷⁹, thereby reducing the number of potential confounding
693 effects. Propofol is a potent agonist of inhibitory GABA-A receptors, directly
694 activating them as well as increasing their affinity for agonists ^{33,34}, leading to
695 suppressed neuronal activity. Propofol also blocks Na⁺ channels, inhibiting
696 glutamate release ¹⁸⁰ and more broadly it inhibits neurotransmitter release at
697 presynaptic terminals ¹⁸¹. There is also some evidence that it may affect the
698 dopaminergic system ^{51,182,183}. Here, we included two independent propofol datasets.
699

700 Western University dataset: Recruitment

701 The Western University ("Western") propofol data were collected between May and
702 November 2014 at the Robarts Research Institute, Western University, London,
703 Ontario (Canada), and have been published before ^{18,144,184,185}. The study received
704 ethical approval from the Health Sciences Research Ethics Board and Psychology
705 Research Ethics Board of Western University (Ontario, Canada). Healthy volunteers
706 (n=19) were recruited (18–40 years; 13 males). Volunteers were right-handed, native
707 English speakers, and had no history of neurological disorders. In accordance with
708 relevant ethical guidelines, each volunteer provided written informed consent, and
709 received monetary compensation for their time. Due to equipment malfunction or

710 physiological impediments to anaesthesia in the scanner, data from n=3 participants
711 (1 male) were excluded from analyses, leaving a total n=16 for analysis ¹⁸.

712 Western University dataset: Study protocol

713 Resting-state fMRI data were acquired at different propofol levels: no sedation
714 (Awake), Deep anaesthesia (corresponding to Ramsay score of 5) and also during
715 post-anaesthetic recovery. As previously reported ¹⁸, for each condition fMRI
716 acquisition began after two anaesthesiologists and one anaesthesia nurse
717 independently assessed Ramsay level in the scanning room. The anaesthesiologists
718 and the anaesthesia nurse could not be blinded to experimental condition, since part
719 of their role involved determining the participants' level of anaesthesia. Note that the
720 Ramsay score is designed for critical care patients, and therefore participants did not
721 receive a score during the Awake condition before propofol administration: rather,
722 they were required to be fully awake, alert and communicating appropriately. To
723 provide a further, independent evaluation of participants' level of responsiveness,
724 they were asked to perform two tasks: a test of verbal memory recall, and a
725 computer-based auditory target-detection task. Wakefulness was also monitored
726 using an infrared camera placed inside the scanner.

727 Propofol was administered intravenously using an AS50 auto syringe infusion pump
728 (Baxter Healthcare, Singapore); an effect-site/plasma steering algorithm combined
729 with the computer-controlled infusion pump was used to achieve step-wise sedation
730 increments, followed by manual adjustments as required to reach the desired target
731 concentrations of propofol according to the TIVA Trainer (European Society for
732 Intravenous Anaesthesia, eurosiva.eu) pharmacokinetic simulation program. This
733 software also specified the blood concentrations of propofol, following the Marsh 3-
734 compartment model, which were used as targets for the pharmacokinetic model
735 providing target-controlled infusion. After an initial propofol target effect-site
736 concentration of $0.6 \mu\text{g mL}^{-1}$, concentration was gradually increased by increments
737 of $0.3 \mu\text{g mL}^{-1}$, and Ramsay score was assessed after each increment: a further
738 increment occurred if the Ramsay score was lower than 5. The mean estimated
739 effect-site and plasma propofol concentrations were kept stable by the
740 pharmacokinetic model delivered via the TIVA Trainer infusion pump. Ramsay level
741 5 was achieved when participants stopped responding to verbal commands, were

742 unable to engage in conversation, and were rousable only to physical stimulation.
743 Once both anaesthesiologists and the anaesthesia nurse all agreed that Ramsay
744 sedation level 5 had been reached, and participants stopped responding to both
745 tasks, data acquisition was initiated. The mean estimated effect-site propofol
746 concentration was 2.48 (1.82- 3.14) $\mu\text{g mL}^{-1}$, and the mean estimated plasma
747 propofol concentration was 2.68 (1.92- 3.44) $\mu\text{g mL}^{-1}$. Mean total mass of propofol
748 administered was 486.58 (373.30- 599.86) mg. These values of variability are typical
749 for the pharmacokinetics and pharmacodynamics of propofol. Oxygen was titrated to
750 maintain SpO₂ above 96%.

751 At Ramsay 5 level, participants remained capable of spontaneous cardiovascular
752 function and ventilation. However, the sedation procedure did not take place in a
753 hospital setting; therefore, intubation during scanning could not be used to ensure
754 airway security during scanning. Consequently, although two anaesthesiologists
755 closely monitored each participant, scanner time was minimised to ensure return to
756 normal breathing following deep sedation. No state changes or movement were
757 noted during the deep sedation scanning for any of the participants included in the
758 study ¹⁸. Propofol was discontinued following the deep anaesthesia scan, and
759 participants reached level 2 of the Ramsey scale approximately 11 minutes
760 afterwards, as indicated by clear and rapid responses to verbal commands. This
761 corresponds to the “recovery” period.

762 As previously reported ¹⁸, once in the scanner participants were instructed to relax
763 with closed eyes, without falling asleep. Resting-state functional MRI in the absence
764 of any tasks was acquired for 8 minutes for each participant. A further scan was also
765 acquired during auditory presentation of a plot-driven story through headphones (5-
766 minute long). Participants were instructed to listen while keeping their eyes closed.
767 The present analysis focuses on the resting-state data only; the story scan data have
768 been published separately ¹⁸⁶ and will not be discussed further here.

769 Western University dataset: MRI Data Acquisition

770 As previously reported ¹⁸, MRI scanning was performed using a 3-Tesla Siemens
771 Tim Trio scanner (32-channel coil), and 256 functional volumes (echo-planar images,
772 EPI) were collected from each participant, with the following parameters: slices = 33,

773 with 25% inter-slice gap; resolution = 3mm isotropic; TR = 2000ms; TE = 30ms; flip
774 angle = 75 degrees; matrix size = 64x64. The order of acquisition was interleaved,
775 bottom-up. Anatomical scanning was also performed, acquiring a high-resolution T1-
776 weighted volume (32-channel coil, 1mm isotropic voxel size) with a 3D MPRAGE
777 sequence, using the following parameters: TA = 5min, TE = 4.25ms, 240x256 matrix
778 size, 9 degrees flip angle ¹⁸.

779 Cambridge University dataset: Recruitment

780 The Cambridge University (“Cambridge”) propofol dataset is described in detail in a
781 previous publication ⁶⁶. Sixteen healthy volunteer subjects were initially recruited for
782 scanning. In addition to the original 16 volunteers, data were acquired for nine
783 additional participants using the same procedures, bringing the total number of
784 participants in this dataset to 25 (11 males, 14 females; mean age 34.7 years, SD =
785 9.0 years). Ethical approval for these studies was obtained from the Cambridgeshire
786 2 Regional Ethics Committee, and all subjects gave informed consent to participate
787 in the study. Volunteers were informed of the risks of propofol administration, such
788 as loss of consciousness, respiratory and cardiovascular depression. They were also
789 informed about more minor effects of propofol such as pain on injection, sedation
790 and amnesia. In addition, standard information about intravenous cannulation, blood
791 sampling and MRI scanning was provided.

792

793 Cambridge University dataset: Study protocol

794 Three target plasma levels of propofol were used - no drug (Awake), 0.6 mg/ml (Mild
795 sedation) and 1.2 mg/ml (Moderate sedation). Scanning (rs-fMRI) was acquired at
796 each stage, and also at Recovery; anatomical images were also acquired. The level
797 of sedation was assessed verbally immediately before and after each of the
798 scanning runs. Propofol was administered intravenously as a “target controlled
799 infusion” (plasma concentration mode), using an Alaris PK infusion pump
800 (Carefusion, Basingstoke, UK). A period of 10 min was allowed for equilibration of
801 plasma and effect-site propofol concentrations. Blood samples were drawn towards
802 the end of each titration period and before the plasma target was altered, to assess

803 plasma propofol levels. In total, 6 blood samples were drawn during the study. The
804 mean (SD) measured plasma propofol concentration was 304.8 (141.1) ng/ml during
805 mild sedation, 723.3 (320.5) ng/ml during moderate sedation and 275.8 (75.42)
806 ng/ml during recovery. Mean (SD) total mass of propofol administered was 210.15
807 (33.17) mg, equivalent to 3.0 (0.47) mg/kg. Two senior anaesthetists were present
808 during scanning sessions and observed the subjects throughout the study from the
809 MRI control room and on a video link that showed the subject in the scanner.
810 Electrocardiography and pulse oximetry were performed continuously, and
811 measurements of heart rate, non-invasive blood pressure, and oxygen saturation
812 were recorded at regular intervals.

813

814 Cambridge University dataset: MRI Data Acquisition

815 The acquisition procedures are described in detail in the original study ³⁷. Briefly,
816 MRI data were acquired on a Siemens Trio 3T scanner (WBIC, Cambridge). For
817 each level of sedation, 150 rs-fMRI volumes (5 min scanning) were acquired. Each
818 functional BOLD volume consisted of 32 interleaved, descending, oblique axial
819 slices, 3 mm thick with interslice gap of 0.75 mm and in-plane resolution of 3 mm,
820 field of view = 192x192 mm, repetition time = 2000 ms, acquisition time = 2 s, time
821 echo = 30 ms, and flip angle 78. T1-weighted structural images at 1 mm isotropic
822 resolution were also acquired in the sagittal plane, using an MPRAGE sequence with
823 TR = 2250 ms, TI = 900 ms, TE = 2.99 ms and flip angle = 9 degrees, for localization
824 purposes. During scanning, volunteers were instructed to close their eyes and think
825 about nothing in particular throughout the acquisition of the resting state BOLD data.
826 Of the 25 healthy subjects, 15 were ultimately retained (7 males, 8 females): 10 were
827 excluded, either because of missing scans (n=2), or due of excessive motion in the
828 scanner (n=8, 5mm maximum motion threshold). For the analyses presented in this
829 paper, we only considered the Awake, Moderate (i.e., loss of behavioural
830 responsiveness) and Recovery resting-state scans.

831

832 Sevoflurane

833 Sevoflurane is an inhalational anaesthetic: specifically, a halogenated ether.
834 Although its exact molecular mechanisms of action are yet to be fully elucidated, in
835 vivo and in vitro evidence indicates that it acts primarily via GABA-A receptors^{2,35–38},
836 but also interacts with NMDA, AMPA^{39,187,188} and nicotinic ACh receptors^{189,190}.
837 Additionally, electrophysiologic investigation suggests possible affinity for as well as
838 Na⁺, K⁺ and hyperpolarization-activated cyclic nucleotide-gated (HCN) channels¹⁹¹.

839

840 Sevoflurane dataset: Recruitment

841 The data included here have been published before^{65,192–194}, and we refer the reader
842 to the original publication for details⁶⁵. The ethics committee of the medical school of
843 the Technische Universität München (München, Germany) approved the current
844 study, which was conducted in accordance with the Declaration of Helsinki. Written
845 informed consent was obtained from volunteers at least 48 h before the study
846 session. Twenty healthy adult men (20 to 36 years of age; mean, 26 years) were
847 recruited through campus notices and personal contact, and compensated for their
848 participation in the study.

849 Before inclusion in the study, detailed information was provided about the protocol
850 and risks, and medical history was reviewed to assess any previous neurologic or
851 psychiatric disorder. A focused physical examination was performed, and a resting
852 electrocardiogram was recorded. Further exclusion criteria were the following:
853 physical status other than American Society of Anesthesiologists physical status I,
854 chronic intake of medication or drugs, hardness of hearing or deafness, absence of
855 fluency in German, known or suspected disposition to malignant hyperthermia, acute
856 hepatic porphyria, history of halothane hepatitis, obesity with a body mass index
857 more than 30 kg/m², gastrointestinal disorders with a disposition for
858 gastroesophageal regurgitation, known or suspected difficult airway, and presence of
859 metal implants. Data acquisition took place between June and December 2013.

860

861 Sevoflurane dataset: Study protocol

862 Sevoflurane concentrations were chosen so that subjects tolerated artificial
863 ventilation (reached at 2.0 vol%) and that burst-suppression (BS) was reached in all
864 participants (around 4.4 vol%). To make group comparisons feasible, an
865 intermediate concentration of 3.0 vol% was also used. In the MRI scanner,
866 volunteers were in a resting state with eyes closed for 700s. Since EEG data were
867 simultaneously acquired during MRI scanning⁶⁵ (though they are not analysed in the
868 present study), visual online inspection of the EEG was used to verify that
869 participants did not fall asleep during the pre-anaesthesia baseline scan.
870 Sevoflurane mixed with oxygen was administered via a tight-fitting facemask using
871 an fMRI-compatible anaesthesia machine (Fabius Tiro, Dräger, Germany). Standard
872 American Society of Anesthesiologists monitoring was performed: concentrations of
873 sevoflurane, oxygen and carbon dioxide, were monitored using a cardiorespiratory
874 monitor (DatexaS/3, General electric, USA). After administering an end-tidal
875 sevoflurane concentration (etSev) of 0.4 vol% for 5 min, sevoflurane concentration
876 was increased in a stepwise fashion by 0.2 vol% every 3 min until the participant
877 became unconscious, as judged by the loss of responsiveness (LOR) to the
878 repeatedly spoken command “squeeze my hand” two consecutive times.
879 Sevoflurane concentration was then increased to reach an end-tidal concentration of
880 approximately 3 vol%. When clinically indicated, ventilation was managed by the
881 physician and a laryngeal mask suitable for fMRI (I-gel, Intersurgical, United
882 Kingdom) was inserted. The fraction of inspired oxygen was then set at 0.8, and
883 mechanical ventilation was adjusted to maintain end-tidal carbon dioxide at steady
884 concentrations of 33 ± 1.71 mmHg during BS, 34 ± 1.12 mmHg during 3 vol%, and
885 33 ± 1.49 mmHg during 2 vol% (throughout this article, mean \pm SD). Norepinephrine
886 was given by continuous infusion ($0.1 \pm 0.01 \mu\text{g} \cdot \text{kg}^{-1} \cdot \text{min}^{-1}$) through an
887 intravenous catheter in a vein on the dorsum of the hand, to maintain the mean
888 arterial blood pressure close to baseline values (baseline, 96 ± 9.36 mmHg; BS, $88 \pm$
889 7.55 mmHg; 3 vol%, 88 ± 8.4 mmHg; 2 vol%, 89 ± 9.37 mmHg; follow-up, 98 ± 9.41
890 mmHg). After insertion of the laryngeal mask airway, sevoflurane concentration was
891 gradually increased until the EEG showed burst-suppression with suppression
892 periods of at least 1,000 ms and about 50% suppression of electrical activity
893 (reached at 4.34 ± 0.22 vol%), which is characteristic of deep anaesthesia. At that

894 point, another 700s of electroencephalogram and fMRI was recorded. Further 700s
895 of data were acquired at steady end-tidal sevoflurane concentrations of 3 and 2
896 vol%, respectively, each after an equilibration time of 15 min. In a final step, etSev
897 was reduced to two times the concentration at LOR. However, most of the subjects
898 moved or did not tolerate the laryngeal mask any more under this condition:
899 therefore, this stage was not included in the analysis ⁶⁵.

900 Sevoflurane administration was then terminated, and the scanner table was slid out
901 of the MRI scanner to monitor post-anaesthetic recovery. The volunteer was
902 manually ventilated until spontaneous ventilation returned. The laryngeal mask was
903 removed as soon as the patient opened his mouth on command. The physician
904 regularly asked the volunteer to squeeze their hand: recovery of responsiveness was
905 noted to occur as soon as the command was followed. Fifteen minutes after the time
906 of recovery of responsiveness, the Brice interview was administered to assess for
907 awareness during sevoflurane exposure; the interview was repeated on the phone
908 the next day. After a total of 45 min of recovery time, another resting-state combined
909 fMRI-EEG scan was acquired (with eyes closed, as for the baseline scan). When
910 participants were alert, oriented, cooperative, and physiologically stable, they were
911 taken home by a family member or a friend appointed in advance.

912

913 Sevoflurane dataset: MRI Data Acquisition

914 Although the original study acquired both functional MRI (fMRI) and
915 electroencephalographic (EEG) data, in the present work we only considered the
916 fMRI data. Data acquisition was carried out on a 3-Tesla magnetic resonance
917 imaging scanner (Achieva Quasar Dual 3.0T 16CH, The Netherlands) with an eight-
918 channel, phased-array head coil. The data were collected using a gradient echo
919 planar imaging sequence (echo time = 30 ms, repetition time (TR) = 1.838 s, flip
920 angle = 75°, field of view = 220 × 220 mm², matrix = 72 × 72, 32 slices, slice
921 thickness = 3 mm, and 1 mm interslice gap; 700-s acquisition time, resulting in 350
922 functional volumes). The anatomical scan was acquired before the functional scan
923 using a T1-weighted MPRAGE sequence with 240 × 240 × 170 voxels (1×1×1 mm
924 voxel size) covering the whole brain. A total of 16 volunteers completed the full

925 protocol and were included in our analyses; one subject was excluded due to high
926 motion, leaving N=15 for analysis. Here, we used fMRI data from the Awake, 3% vol,
927 and Recovery scans.

928

929 Ketamine

930 Ketamine is a multi-faceted drug, in terms of both neurophysiology and how it affects
931 subjective experience. Depending on dosage, it can act as a “dissociative”
932 anaesthetic (high dose) or as an “atypical psychedelic” (at sub-anaesthetic dose) ^{40–}
933 ⁴⁴. At small doses, it has also found recent use as a fast-acting antidepressant ^{195,196}.
934 Both the anaesthetic and psychedelic effects of ketamine are in some respect
935 unusual; unlike widely used anaesthetics like propofol and sevoflurane, ketamine
936 does not exert its anaesthetic function through agonism of GABA receptors, nor does
937 it recruit sleep-promoting hypothalamic nuclei, which it appears to suppress instead
938 ^{24,43}. Likewise, although ketamine does induce psychedelic-like symptoms such as
939 perceptual distortions, vivid imagery and hallucinations, like classic psychedelics, it
940 also induces prominent dissociative symptoms of disembodiment ^{43,63,197–199}. Its
941 psychedelic action is not mediated by the serotonin 2A receptor, on which classic
942 psychedelics operate ^{46,49}: although its precise mechanisms of action are yet to be
943 fully elucidated, ketamine appears to be primarily an antagonist of NMDA and HCN1
944 receptors; however, evidence suggests that cholinergic, aminergic, and opioid
945 systems may also play modulatory roles ^{44,45,50}.

946

947 Ketamine dataset: Recruitment

948 The ketamine data included in this study have been published before ⁶³, and we refer
949 the reader to the original publication for details. Briefly, a total of 21 participants (10
950 males; mean age 28.7 years, SD = 3.2 years) were recruited via advertisements
951 placed throughout central Cambridge, UK ⁶³. All participants underwent a screening
952 interview in which they were asked whether they had previously been diagnosed or
953 treated for any mental health problems and whether they had ever taken any
954 psychotropic medications. Participants reporting a personal history of any mental

955 health problems or a history of any treatment were excluded from the study. All
956 participants were right-handed, were free of current of previous psychiatric or
957 neurological disorder or substance abuse problems, and had no history of
958 cardiovascular illness or family history of psychiatric disorder/substance abuse. The
959 study was approved by the Cambridge Local Research and Ethics Committee, and
960 all participants provided written informed consent in accordance with ethics
961 committee guidelines.

962

963 Ketamine dataset: Study protocol

964 Participants were scanned (resting-state functional MRI and anatomical T1) on two
965 occasions, separated by at least 1 week. On one occasion, they received a
966 continuous computer-controlled intravenous infusion of a racemic ketamine solution
967 (2 mg/ml) until a targeted plasma concentration of 100 ng/ml was reached. This
968 concentration was sustained throughout the protocol. A saline infusion was
969 administered on the other occasion. Infusion order was randomly counterbalanced
970 across participants. The infusion was performed and monitored by a trained
971 anaesthetist (R.A.) who was unblinded for safety reasons, but who otherwise had
972 minimal contact with participants. At all other times, participants were supervised by
973 investigators blinded to the infusion protocol. The participants remained blinded until
974 both assessments were completed. Bilateral intravenous catheters were inserted into
975 volunteers' forearms, one for infusion, and the other for serial blood sampling. A
976 validated and previously implemented²⁰⁰ three-compartment pharmacokinetic model
977 was used to achieve a constant plasma concentration of 100 ng/ml using a
978 computerized pump (Graseby 3500, Graseby Medical, UK). The infusion continued
979 for 15 min to allow stabilization of plasma levels. Blood samples were drawn before
980 and after the resting fMRI scan and then placed on ice. Plasma was obtained by
981 centrifugation and stored at -70 °C. Plasma ketamine concentrations were measured
982 by gas chromatography–mass spectrometry.

983

984 Ketamine dataset: MRI Data Acquisition

985 All MRI and assessment procedures were identical across assessment occasions.
986 Scanning was performed using a 3.0 T MRI scanner (Siemens Magnetom, Trio Tim,
987 Erlangen, Germany) equipped with a 12-channel array coil located at the Wolfson
988 Brain Imaging Centre, Addenbrooke's Hospital, Cambridge, UK. T2*-weighted echo-
989 planar images were acquired under eyes-closed resting-state conditions.
990 Participants were instructed to close their eyes and let the minds wander without
991 going to sleep. Subsequent participant debriefing ensured that no participants fell
992 asleep during the scan. Imaging parameters were: 3x3x3.75mm voxel size, with a
993 time-to-repetition (TR) of 2000 ms, time-to-echo (TE) of 30 ms, flip angle of 781 in
994 64x64 matrix size, and 240mm field of view (FOV). A total of 300 volumes
995 comprising 32 slices each were obtained. In addition, high- resolution anatomical T1
996 images were acquired using a three-dimensional magnetic-prepared rapid gradient
997 echo (MPPRAGE) sequence. In all, 176 contiguous sagittal slices of 1.0mm
998 thickness using a TR of 2300 ms, TE of 2.98 ms, flip angle of 91, and a FOV of
999 256mm in 240x256 matrix were acquired with a voxel size of 1.0mm³. One
1000 participant was excluded due to excessive movement, resulting in a final sample of
1001 N=20 subjects.

1002

1003 LSD

1004 LSD (lysergic acid diethylamide) is perhaps the best-known among classic
1005 psychedelics, inducing a powerful state of altered consciousness with subjective
1006 experiences including hallucinations and “ego dissolution”^{46,48,49}. Substantial work in
1007 humans and animals has demonstrated that LSD influences neuromodulation,
1008 having affinity for multiple receptors, primarily serotonergic (5-HT_{2A}, 5-HT_{1A/B}, 5-
1009 HT₆, 5-HT₇) and dopaminergic (D₁ and D₂ receptors)^{46,48,52,201,202}.

1010 The main neural and subjective effects of LSD originate from its agonism of the 5-
1011 HT_{2A} receptor: both effects are abolished by pre-treatment with the non-selective
1012 5HT₂ antagonist ketanserin, which has highest affinity for the 5HT_{2A} receptor^{168,203}.
1013 In humans, functional connectivity under LSD shows significant correspondence with
1014 the spatial distribution of the 5HT_{2A} receptor²⁰⁴. Providing evidence for a
1015 mechanistic role, both PET maps and transcriptomic maps of the 5HT_{2A} receptor

1016 (but not other serotonin receptors) have been shown to improve the ability of
1017 computational models to recapitulate the effects of LSD on brain activity and
1018 connectivity, as measured by fMRI ^{71,72,175}. Therefore, pharmacological and in silico
1019 evidence converge towards the central role of the 5HT2A receptor for LSD's ability to
1020 alter consciousness and its neural underpinnings – although other receptors have
1021 also been shown to play an auxiliary role ⁵².

1022

1023 LSD dataset: Recruitment

1024 The LSD data employed here have been extensively published, and we refer to the
1025 original publication for details ⁶⁰. Briefly, collection of these data ⁶⁰ was approved by
1026 the National Research Ethics Service Committee London–West London and was
1027 conducted in accordance with the revised declaration of Helsinki (2000), the
1028 International Committee on Harmonization Good Clinical Practice guidelines and
1029 National Health Service Research Governance Framework. Imperial College London
1030 sponsored the research, which was conducted under a Home Office license for
1031 research with schedule 1 drugs. All participants were recruited via word of mouth
1032 and provided written informed consent to participate after study briefing and
1033 screening for physical and mental health. The screening for physical health included
1034 electrocardiogram (ECG), routine blood tests, and urine test for recent drug use and
1035 pregnancy. A psychiatric interview was conducted and participants provided full
1036 disclosure of their drug use history. Key exclusion criteria included: < 21 years of
1037 age, personal history of diagnosed psychiatric illness, immediate family history of a
1038 psychotic disorder, an absence of previous experience with a classic psychedelic
1039 drug (e.g. LSD, mescaline, psilocybin/magic mushrooms or DMT/ayahuasca), any
1040 psychedelic drug use within 6 weeks of the first scanning day, pregnancy,
1041 problematic alcohol use (i.e. > 40 units consumed per week), or a medically
1042 significant condition rendering the volunteer unsuitable for the study. Twenty healthy
1043 volunteers with previous experience using psychedelic drugs were scanned.

1044

1045 LSD dataset: Study protocol

1046 Volunteers underwent two scans, 14 days apart. On one day they were given a
1047 placebo (10-mL saline) and the other they were given an active dose of LSD (75 μ g
1048 of LSD in 10-mL saline). The order of the conditions was balanced across
1049 participants, and participants were blind to this order but the researchers were not.
1050 Participants carried out VAS-style ratings via button-press and a digital display
1051 screen presented after each scan, and the 11-factor altered states of conscious-
1052 ness (ASC) questionnaire was completed at the end of each dosing day ⁶⁰. All
1053 participants reported marked alterations of consciousness under LSD.

1054 The data acquisition protocols were described in detail in the original publication ⁶⁰,
1055 so we will only describe them in brief here. The infusion (drug/placebo) was
1056 administered over 2 min and occurred 115 min before the resting-state scans were
1057 initiated. After infusion, subjects had a brief acclimation period in a mock MRI
1058 scanner to prepare them for the experience of being in the real machine. ASL and
1059 BOLD scanning consisted of three seven-minute eyes closed resting state scans.
1060 The ASL data were not analysed for this study, and will not be discussed further.

1061

1062 LSD dataset: MRI Data Acquisition

1063 The first and third scans were eyes-closed, resting state without stimulation, while
1064 the second scan involved listening to music; however, this scan was not used in this
1065 analysis. The precise length of each of the two BOLD scans included here was 7:20
1066 minutes. For the present analysis, these two scans were concatenated together in
1067 time. Imaging was performed on a 3T GE HDx system. High-resolution anatomical
1068 images were acquired with 3D fast spoiled gradient echo scans in an axial
1069 orientation, with field of view = 256x256x192 and matrix = 256x256x129 to yield
1070 1mm isotropic voxel resolution. TR/TE = 7.9/3.0ms; inversion time = 450ms; flip
1071 angle = 20. BOLD-weighted fMRI data were acquired using a gradient echo planer
1072 imaging sequence, TR/TE = 2000/35ms, FoV = 220mm, 64x64 acquisition matrix,
1073 parallel acceleration factor = 2, 90 flip angle. Thirty five oblique axial slices were
1074 acquired in an interleaved fashion, each 3.4mm thick with zero slice gap (3.4mm
1075 isotropic voxels). One subject aborted the experiment due to anxiety and four others
1076 were excluded for excessive motion (measured in terms of frame-wise

1077 displacement), leaving 15 subjects for analysis (11 males, 4 females; mean age 30.5
1078 years, SD = 8.0 years) ⁶⁰.

1079

1080 Ayahuasca

1081 The Amazonian beverage ayahuasca is typically used in shamanic religious rituals,
1082 where it is obtained as a tea made from two plants: *Psychotria viridis* and
1083 *Banisteriopsis caapi*. *Psychotria viridis* contains the tryptamine N,N-di-
1084 methyltryptamine (DMT), which binds to sigma-1 and serotonin (particularly 2A)
1085 receptors ^{210,211}. *Banisteriopsis caapi* contains beta-carboline alkaloids, notably
1086 harmine, tetrahydroharmine (THH), and harmaline. As potent monoamine oxidase
1087 inhibitors (MAOI), harmine and harmaline prevent the degradation of monoamine
1088 neurotransmitters and thus increase their levels; and THH acts as a mild selective
1089 serotonin reuptake inhibitor and a weak MAOI ^{212–214}.

1090 Ayahuasca dataset: Recruitment

1091 The ayahuasca data that we used have been published before ^{62,137}, and we refer
1092 the reader to the original publication for details. Briefly, data were obtained from 9
1093 healthy right-handed adult volunteers (mean age 31.3, from 24 to 47 years), all who
1094 were experienced users of Ayahuasca with at least 5 years use (twice a month) and
1095 at least 8 years of formal education. The experimental procedure was approved by
1096 the Ethics and Research Committee of the University of São Paulo at Ribeirão Preto
1097 (process number 14672/2006). Written informed consent was obtained from all
1098 volunteers, who belonged to the Santo Daime religious organisation. All
1099 experimental procedures were performed in accordance with the relevant guidelines
1100 and regulations. Volunteers were not under medication for at least 3 months prior to
1101 the scanning session and were abstinent from caffeine, nicotine and alcohol prior to
1102 the acquisition. They had no history of neurological or psychiatric disorders, as
1103 assessed by DSM-IV structured interview⁷¹. Subjects ingested 120–200 mL (2.2
1104 mL/kg of body weight) of Ayahuasca known to contain 0.8 mg/mL of DMT and 0.21
1105 mg/mL of harmine. Harmaline was not detected via the chromatography analysis, at
1106 the threshold of 0.02 mg/mL⁷.

1107

1108 Ayahuasca dataset: Study protocol

1109 Volunteers underwent two distinct fMRI scanning sessions: (i) before and (ii) 40
1110 minutes after Ayahuasca intake, when the subjective effects become noticeable (the
1111 volunteers drank 2.2 mL/kg of body weight and the Ayahuasca contained 0.8 mg/mL
1112 of DMT and 0.21 mg/mL of harmine, see Methods section). In both cases,
1113 participants were instructed to close their eyes and remain awake and at rest,
1114 without performing any task.

1115

1116 Ayahuasca dataset: MRI Data Acquisition

1117 The fMRI images were obtained in a 1.5 T scanner (Siemens, Magnetom Vision),
1118 using an EPI-BOLD like sequence comprising 150 volumes, with the following
1119 parameters: TR = 1700 ms; TE = 66 ms; FOV = 220 mm; matrix 64 × 64; voxel
1120 dimensions of 1.72 mm × 1.72 mm × 1.72 mm. Whole brain high resolution T1-
1121 weighted images were also acquired (156 contiguous sagittal slices) using a
1122 multiplanar reconstructed gradient-echo sequence, with the following parameters:
1123 TR = 9.7 ms; TE = 44 ms; flip angle 12°; matrix 256 × 256; FOV = 256 mm, voxel
1124 size = 1 mm × 1 mm × 1 mm. Data from one volunteer were excluded from analyses
1125 due to acquisition limitations resulting in incomplete brain coverage. The final dataset
1126 included 8 subjects.

1127

1128 Modafinil

1129 Modafinil is a wakefulness promoting drug used for the treatment of sleep disorders
1130 such as narcolepsy (under the commercial name Provigil), as well as finding use as
1131 a cognitive enhancer for attention and memory ^{6,7,64}, and to combat the cognitive
1132 symptoms of Attention Deficit/Hyperactivity Disorder (ADHD), and mood disorders,
1133 owing to its lower addiction risk in comparison with amphetamine-like
1134 psychostimulants ^{6-9,215}. This drug has a broad neurotransmitter profile: it acts as a
1135 blocker of the dopamine and noradrenaline transporters, as well as modulating locus

1136 coeruleus noradrenergic firing, and acting on the wake-promoting hypothalamic
1137 neuropeptide orexin to activate the histamine system; it also influences both the
1138 glutamate and GABA systems ^{8,216–220}.

1139

1140 Modafinil dataset: Recruitment

1141 The modafinil dataset has been published before ^{64,221}. As reported in the original
1142 publication, the study was approved by the ethics committee of University of Chieti
1143 (PROT 2008/09 COET on 14/10/2009) and conducted in accordance with the
1144 Helsinki Declaration. The study design was explained in detail and written informed
1145 consent was obtained from all participants involved in our study. Recruitment was
1146 performed throughout February 2011, drug/placebo administration and fMRI
1147 acquisitions started on March 2011, went on until January 2012, and the study was
1148 completed with the last fMRI session in January 2012. After securing financial
1149 coverage for costs related to the analysis of the study, the trial was registered on
1150 10/09/2012 (ClinicalTrials.gov
1151 NCT01684306<http://clinicaltrials.gov/ct2/show/NCT01684306>). After obtaining
1152 registration, the double-blind study was opened and analyzed.

1153 This dataset was obtained from the OpenfMRI database. Its accession number is
1154 ds000133. A total of twenty six young male right-handed (as assessed by the
1155 EdinburghHandedness inventory) adults (age range: 25–35 years) with comparable
1156 levels of education (13 years) were enrolled. All subjects had no past or current
1157 signs of psychiatric, neurological or medical (hypertension, cardiac disorders,
1158 epilepsy) conditions as determined by the Millon test and by clinical examination.
1159 Subjects showing visual or motor impairments were excluded as well as individuals
1160 taking psychoactive drugs or having a history of alcohol abuse. All volunteers were
1161 instructed to maintain their usual amount of nicotine and caffeine intake and avoid
1162 alcohol consumption in the 12h before the initiation of the study.

1163

1164 Modafinil dataset: Study protocol

1165 Study subjects received, in a double blind fashion, either a single dose of modafinil
1166 (100 mg) (modafinil group; N=13) or a placebo (placebo group; N=13) pill identical to
1167 the drug. Randomization of study subjects was obtained by means of a random
1168 number generator. Here, we only considered data from the modafinil group. The day
1169 after drug/placebo assumption, subjects were asked about perceived side effects
1170 and, in particular, sleep disturbances. All but one reported no modafinil-induced side-
1171 effects or alterations in the sleep-wake cycle. Rs-fMRI BOLD data were separated in
1172 three runs lasting four minutes each followed by high resolution T1 anatomical
1173 images. Two scanning sessions took place: one before ingesting the drug/placebo,
1174 and one 3 hours later, to account for pharmacokinetics. Subjects were asked to relax
1175 while fixating the central point in the middle of a grey-background screen that was
1176 projected on an LCD screen and viewed through a mirror placed above the subject's
1177 head. Subject head was positioned within an eight-channel coil and foam padding
1178 was employed to minimize involuntary head movements.

1179

1180 Modafinil dataset: MRI Data Acquisition

1181 BOLD functional imaging was performed with a Philips Achieva 3T Scanner (Philips
1182 Medical Systems, Best, The Netherlands), using T2*-weighted echo planar imaging
1183 (EPI) free induction decay (FID) sequences and applying the following parameters:
1184 TE 35 ms, matrix size 64x64, FOV 256 mm, in-plane voxel size 464 mm, flip angle
1185 75 degrees, slice thickness 4 mm and no gaps. 140 functional volumes consisting of
1186 30 transaxial slices were acquired per run with a volume TR of 1,671 ms. High-
1187 resolution structural images were acquired at the end of the three rs-fMRI runs
1188 through a 3D MPRAGE sequence employing the following parameters: sagittal,
1189 matrix 256x256, FOV 256 mm, slice thickness 1 mm, no gaps, in-plane voxel size 1
1190 mm x 1 mm, flip angle 12 degrees, TR = 9.7 ms and TE = 4 ms. Two subjects from
1191 the modafinil group were excluded from analysis due to acquisition limitations,
1192 leaving N=11 subjects for analysis.

1193

1194 Methylphenidate

1195 Methylphenidate is used as a cognitive enhancer to treat the cognitive symptoms of
1196 ADHD and narcolepsy (under the name Ritalin)^{4,11}. Pharmacologically, it inhibits the
1197 reuptake of both dopamine and noradrenaline by blocking their transporters;
1198 although yet to be conclusively confirmed, there is also in vitro evidence suggesting
1199 an additional minor affinity of methylphenidate for the 5-HT_{1A} receptor^{222–228}.

1200

1201 Methylphenidate dataset: Recruitment

1202 The methylphenidate dataset used here has been published before^{10,51}. Unlike the
1203 other datasets included in this study, the methylphenidate data were not obtained
1204 from healthy controls, but rather from a cohort of patients suffering from traumatic
1205 brain injury (TBI). Volunteers with a history of moderate to severe traumatic brain
1206 injury (inclusion criteria: age 18–60 years and not recruited to more than three
1207 research studies within the calendar year) were referred from the Addenbrooke's
1208 Neurosciences Critical Care Unit Follow-Up Clinic, Addenbrooke's Traumatic Brain
1209 Injury Clinic and The Royal London Hospital Intensive Care Unit (see the original
1210 publication for details of patient injuries). The patients were sent a written invitation
1211 to take part in the study. All volunteers gave written informed consent before
1212 participating in the study.

1213 Thirty-eight volunteers were recruited to the study; 17 (12 male, 5 female) into the
1214 TBI arm of the study and 21 (13 male, 8 female) into the healthy control (HC) arm of
1215 the study. Exclusion criteria included National Adult Reading Test (NART) <70, Mini
1216 Mental State Examination (MMSE) <23, left-handedness, history of drug/alcohol
1217 abuse, history of psychiatric or neurological disorders, contraindications for MRI
1218 scanning, medication that may affect cognitive performance or prescribed for
1219 depression, and any physical handicap that could prevent the completion of testing.

1220 Our sample contains mostly patients with diffuse axonal injuries and small lesions.
1221 The patients were at least 6 months post TBI. Four sustained moderate TBI with a
1222 score of between 9 and 12 on the Glasgow Coma Scale (GCS) and 11 sustained

1223 severe TBI with a GCS score of 8 or below on presentation. The mean age of the
1224 patient group was 36 years (± 13 years).

1225

1226 Methylphenidate dataset: Study protocol

1227 The study consisted of two visits (separated by 2–4 weeks) for both groups of
1228 participants. The TBI volunteers were randomly allocated in a Latin square design to
1229 receive one of the two interventions on the first visit (a placebo tablet or 30 mg tablet
1230 of methylphenidate), and the alternate intervention on the second visit. The decision
1231 to use 30 mg of methylphenidate was based on comparable doses used in previous
1232 studies in healthy participants (Gilbert et al., 2006; Marquand et al., 2011; Costa et
1233 al., 2013) as well as NICE guidelines for medication in adults
1234 (www.nice.org.uk) which stipulate that when methylphenidate is titrated for side
1235 effects and responsiveness in each individual subject, the dose should range from a
1236 minimum of 15 mg to a maximum dose of 100 mg. As the dose of methylphenidate
1237 was not calculated by the participant's body weight, an interventional dose at the
1238 lower end of the dose range was chosen, which had also been used in previous
1239 studies (Gilbert et al., 2006; Marquand et al., 2011; Costa et al., 2013; Fallon et al.,
1240 2017). After a delay of 75 min to ensure that peak plasma levels of methylphenidate
1241 were reached, the volunteers completed a MRI scan which included both fMRI and
1242 structural image acquisition. The volunteers attended their two fMRI assessments at
1243 the same time interval as the patients, but without any pharmacological intervention.
1244 Therefore, here we only considered the patient data.

1245

1246 Methylphenidate dataset: MRI Data Acquisition

1247 MRI data were acquired on a Siemens Trio 3-Tesla MR system (Siemens AG,
1248 Munich, Germany). MRI scanning started with the acquisition of a localizer scan and
1249 was followed by a 3D high resolution MPRAGE image [Relaxation Time (TR) 2,300
1250 ms, Echo Time (TE) 2.98 ms, Flip Angle 9°, FOV 256×256 mm²]. Diffusion Tensor
1251 Imaging (DTI) data (63 non-collinear directions, $b=1,000$ s/mm² with one volume
1252 acquired without diffusion weighting ($b=0$), echo time 106ms, repetition time 1,700

1253 ms, field of view 192×192 mm, 2 mm isotropic voxels) were also collected to
1254 investigate white matter integrity. Here, we did not analyse the DTI data.

1255 Functional imaging data were acquired using an echo-planar imaging (EPI)
1256 sequence with parameters TR = 2,000 ms, TE = 30 ms, Flip Angle = 78°, FOV
1257 192×192 mm², in-plane resolution 3.0×3.0 mm, 32 slices 3.0 mm thick with a gap of
1258 0.75 mm between slices. Two patients were excluded from the analysis (one patient
1259 only attended one of the study sessions and the other had excessive movement
1260 artifacts in their fMRI scan), leaving N=15 patients for analysis.

1261

1262 Functional MRI preprocessing and denoising

1263 Preprocessing

1264 The preprocessing and image analysis were performed using the CONN toolbox,
1265 version 17f (CONN; <http://www.nitrc.org/projects/conn>)²²⁹ based on Statistical
1266 Parametric Mapping 12 (<http://www.fil.ion.ucl.ac.uk/spm>), implemented in MATLAB
1267 2016a. For each dataset and condition, we applied a standard preprocessing
1268 pipeline, the same as we employed in our previous studies^{18,21,138,194}. The pipeline
1269 involved the following steps: removal of the first five volumes, to achieve steady-
1270 state magnetization; motion correction; slice-timing correction; identification of outlier
1271 volumes for subsequent scrubbing by means of the quality assurance/artifact
1272 rejection software *art* (http://www.nitrc.org/projects/artifact_detect); normalisation to
1273 Montreal Neurological Institute (MNI-152) standard space (2 mm isotropic
1274 resampling resolution), using the segmented grey matter image from each
1275 volunteer's T1-weighted anatomical image, together with an *a priori* grey matter
1276 template.

1277

1278 Denoising

1279 Denoising was also performed using the CONN toolbox. To reduce noise due to
1280 cardiac and motion artifacts, which are known to impact functional connectivity²³⁰,
1281 we applied the anatomical CompCor (aCompCor) method of denoising the functional

1282 data ²³¹ as implemented within the CONN toolbox. The aCompCor method involves
1283 regressing out of the functional data the first five principal components attributable to
1284 white matter and cerebrospinal fluid (CSF) signal; six subject-specific realignment
1285 parameters (three translations and three rotations) as well as their first-order
1286 temporal derivatives; followed by scrubbing our outliers identified by ART, using
1287 Ordinary Least Squares regression ²²⁹. Finally, the denoised BOLD signal timeseries
1288 were linearly detrended and band-pass filtered to eliminate both low-frequency drift
1289 effects and high-frequency noise, thus retaining frequencies between 0.008 and 0.09
1290 Hz.

1291 The step of global signal regression (GSR) has received substantial attention in the
1292 literature as a denoising method ^{232–234}. GSR mathematically mandates that
1293 approximately 50% of correlations between regions will be negative ²³⁵; however, the
1294 proportion of anticorrelations between brain regions has been shown to vary across
1295 states of consciousness, including anaesthesia and psychedelics ^{18,138}. Indeed,
1296 recent work has demonstrated that the global signal contains information about
1297 states of consciousness ²³⁶. Therefore, in line with our previous studies, here we
1298 decided to avoid GSR in favour of the aCompCor denoising procedure, which is
1299 among those recommended for investigations of dynamic connectivity ²³³.

1300

1301 Summarising pharmacological effects on brain function

1302 For each subject at each condition, the denoised regional BOLD signals were
1303 parcellated into 100 cortical regions according to the local-global functional
1304 parcellation of Schaefer and colleagues ¹⁰⁷. The parcellated regional BOLD signals
1305 were then correlated (“functional connectivity”); after removing negative-valued
1306 edges, the regional strength of functional connectivity (node strength) was measured
1307 for each region. The regional change in FC strength was then quantified for each
1308 subject (for the methylphenidate dataset, this was quantified with respect to the
1309 mean of controls’ node strength values). Finally, for each dataset, we computed the
1310 mean across subjects of the FC strength deltas. Therefore, each pharmacological
1311 intervention was summarised as one vector of regional FC strength deltas (Figure 1).

1312

1313 Receptor maps from Positron Emission Tomography

1314 Receptor densities were estimated using PET tracer studies for a total of 18
1315 receptors and transporters, across 9 neurotransmitter systems, recently made
1316 available by Hansen and colleagues
1317 at https://github.com/netneurolab/hansen_receptors³¹. These include dopamine (D1
1318 ⁷⁴, D2 ^{75–78}, DAT ⁷⁹), norepinephrine (NET ^{80–83}), serotonin (5-HT1A ⁸⁴, 5-HT1B <sup>84–
1319 87,87–89</sup>, 5-HT2A ⁹⁰, 5-HT4 ⁹⁰, 5-HT6 ^{91,92}, 5-HTT ⁹⁰), acetylcholine (α 4 β 2 ^{93,94}, M1 ⁹⁵,
1320 VACHT ^{96,97}), glutamate (mGluR5 ^{98,99}), GABA (GABA-A ¹⁰⁰), histamine (H3 ¹⁰¹),
1321 cannabinoid (CB1 ^{102–105}), and opioid (MOR ¹⁰⁶). Volumetric PET images were
1322 registered to the MNI-ICBM 152 nonlinear 2009 (version c, asymmetric) template,
1323 averaged across participants within each study, then parcellated and
1324 receptors/transporters with more than one mean image of the same tracer (5-HT1b,
1325 D2, VACHT) were combined using a weighted average. See Hansen et al ³¹ for
1326 detailed information about each map and their limitations.

1327

1328 Partial Least Squares Analysis

1329

1330 PLS analysis was used to relate regional neurotransmitter density to
1331 pharmacologically-induced functional connectivity changes. PLS analysis is an
1332 unsupervised multivariate statistical technique that decomposes relationships
1333 between two datasets (in our case, neurotransmitter density with n regions and r
1334 neurotransmitters, $X_{n \times r}$, and drug-induced functional connectivity changes, $Y_{n \times d}$ with n
1335 regions and d drugs) into orthogonal sets of latent variables with maximum
1336 covariance, which are linear combinations of the original data ^{115,116}. In other words,
1337 PLS finds components from the predictor variables (100 \times 18 matrix of regional
1338 neurotransmitter receptor and transporter density scores) that have maximum
1339 covariance with the response variables (100 \times 12 matrix of regional changes in FC
1340 induced by different drugs). The PLS components (i.e., linear combinations of the
1341 weighted neurotransmitter density) are ranked by covariance between predictor and
1342 response variables, so that the first few PLS components provide a low-dimensional
1343 representation of the covariance between the higher dimensional data matrices.
1344 Thus, the first PLS component (PLS1) is the linear combination of the weighted

1345 neurotransmitter density scores that have a brain expression map that covaries the
1346 most with the map of regional FC changes.

1347

1348 This is achieved by z-scoring both data matrices column-wise and applying singular
1349 value decomposition on the matrix $Y'X$, such that:

1350

$$1351 \qquad (Y'X)' = USV' \qquad (1)$$

1352

1353
1354 where U_{gxt} and V_{txt} are orthonormal matrices consisting of left and right singular
1355 vectors and S_{txt} is a diagonal matrix of singular values. The i^{th} columns of U and V
1356 constitute a latent variable, and the i^{th} singular value in S represents the covariance
1357 between singular vectors. The i^{th} singular value is proportional to the amount of
1358 covariance between neurotransmitter density, and drug-induced FC changes
1359 captured by the i^{th} latent variable, where the effect size can be estimated as the ratio
1360 of the squared singular value to the sum of all squared singular values. In the
1361 present study, the left singular vectors (that is, the columns of U) represent the
1362 degree to which each neurotransmitter contributes to the latent variable and
1363 demonstrate the extracted association between neurotransmitter density and drug-
1364 induced FC changes (neurotransmitter weights). The right singular vectors (that is,
1365 the columns of V) represent the degree to which the FC changes contribute to the
1366 same latent variable (term weights). Positively weighed neurotransmitters covary
1367 with positively weighed drug-induced changes, and negatively weighed
1368 neurotransmitters covary with negatively weighed drug-induced changes.

1369

1370 Scores at each brain region for each latent variable can be computed by projecting
1371 the original data onto the singular vector weights. Positively scored brain regions are
1372 regions that demonstrate the covariance between the prevalence of positively
1373 weighted neurotransmitters and positively weighted drug-induced effects (and vice
1374 versa for negatively scored brain regions). Loadings for each variable were
1375 computed as the Pearson's correlation between each individual variable's activity
1376 (neurotransmitter density and drug-induced FC changes) and the PLS analysis-
1377 derived neurotransmitter score pattern. Squaring the loading (a correlation) equals
1378 the percentage variance shared between an original variable and the PLS analysis-

1379 derived latent variable. Variables with high absolute loadings are highly correlated to
1380 the score pattern, indicating a large amount of shared variance between the
1381 individual variable and the latent variable.

1382

1383 We confirmed that PLS1 explained the largest amount of variance by testing across
1384 a range of PLS components (between 1 and 12) and quantifying the relative variance
1385 explained by each component. The statistical significance of the variance explained
1386 by each PLS model was tested by permuting the response variables 1,000 times,
1387 while considering the spatial dependency of the data by using spatial
1388 autocorrelation-preserving permutation tests, termed spin tests^{117–120}. Parcel
1389 coordinates were projected onto the spherical surface and then randomly rotated
1390 and original parcels were reassigned the value of the closest rotated parcel (10,000
1391 repetitions). The procedure was performed at the parcel resolution rather than the
1392 vertex resolution to avoid upsampling the data. In PLS analysis, the spin test is
1393 applied to the singular values (or equivalently, the covariance explained) of the latent
1394 variables, producing a null distribution of singular values. This is done applying PLS
1395 analysis to the original X matrix and a spun Y matrix. The spin test embodies the null
1396 hypothesis that neurotransmitter density and drug-induced FC changes are spatially
1397 correlated with each other only because of inherent spatial autocorrelation. The p -
1398 value is computed as the proportion of null singular values that are greater in
1399 magnitude than the empirical singular values. Thus, these p -values represent the
1400 probability that the observed spatial correspondence between neurotransmitter
1401 density and drug-induced FC changes could occur by randomly correlating maps
1402 with comparable spatial autocorrelation.

1403

1404 Hierarchical organisation

1405

1406 We quantified the spatial similarity of each pharmacologically-induced pattern of
1407 change in FC strength, with several canonical maps of hierarchical brain
1408 organisation (“canonical brain hierarchies”) derived from multimodal neuroimaging.
1409 We considered the anatomical gradient of intracortical myelination obtained from
1410 T1w/T2w MRI ratio⁵⁸; evolutionary cortical expansion obtained by comparing human
1411 and macaque¹²²; the principal component of variation in gene expression from the

1412 Allen Human Brain Atlas transcriptomic database (AHBA; <https://human.brain->
1413 [map.org/](https://human.brain-map.org/)), referred to as “AHBA PC1”^{54,59,123}; the principal component of variation in
1414 task activation from NeuroSynth, (<https://github.com/neurosynth/neurosynth>), an
1415 online meta-analytic tool that synthesizes results from more than 15,000 published
1416 fMRI studies by searching for high-frequency key words that are published alongside
1417 fMRI voxel coordinates, using the volumetric association test maps (referred to as
1418 “NeuroSynth PC1”) ^{54,59,124}; the map of cerebral blood flow ⁵⁴; the principal gradient
1419 of variation in functional connectivity ⁵⁷; and a recently derived gradient of regional
1420 prevalence of different kinds of information, from redundancy to synergy ¹²⁵.

1421

1422 Spatial similarity between brain maps was quantified in terms of Spearman
1423 correlation, and statistical significance was assessed against a spin-based null
1424 model with preserved spatial autocorrelation, as described above ^{117–120}.

1425

1426

1427 ENIGMA cortical vulnerability data

1428

1429 Patterns of cortical thickness were collected for the available 11 neurological,
1430 neurodevelopmental, and psychiatric disorders from the ENIGMA (Enhancing
1431 Neuroimaging Genetics through Meta-Analysis) consortium and the *enigma* toolbox
1432 (<https://github.com/MICA-MNI/ENIGMA>) ¹²⁶: 22q11.2 deletion syndrome (22q) ¹²⁷,
1433 attention-deficit/hyperactivity disorder (ADHD) ¹²⁸, autism spectrum disorder (ASD)
1434 ¹²⁹, idiopathic generalized epilepsy ¹³⁰, right temporal lobe epilepsy ¹³⁰, left temporal
1435 lobe epilepsy ¹³⁰, depression ¹³¹, obsessive-compulsive disorder (OCD) ¹³²,
1436 schizophrenia ¹³³, bipolar disorder (BD) ¹³⁴, and Parkinson’s disease (PD) ¹³⁵. The
1437 ENIGMA consortium is a data-sharing initiative that relies on standardized image
1438 acquisition and processing pipelines, such that disorder maps are comparable ²³⁷.
1439 Altogether, over 21,000 patients were scanned across the thirteen disorders, against
1440 almost 26,000 controls. The values for each map are z-scored effect sizes (Cohen’s
1441 *d*) of cortical thickness in patient populations versus healthy controls. Imaging and
1442 processing protocols can be found at <http://enigma.ini.usc.edu/protocols/>.

1443 For every brain region, we constructed an 11-element vector of disorder abnormality,
1444 where each element represents a disorder’s cortical abnormality at the region. For
1445 every pair of brain regions, we correlated the abnormality vectors to quantify how
1446 similarly two brain regions are affected across disorders. This results in a region-by-
1447 region matrix of “disorder co-susceptibility” ¹⁰⁹.

1448
1449

1450 Acknowledgements

1451

1452 This work was carried out thanks to support from the Gates Cambridge Trust (OPP 1144) [to
1453 ALL]; the Wellcome Trust Research Training Fellowship (grant no. 083660/Z/07/Z), Raymond
1454 and Beverly Sackler Studentship, and the Cambridge Commonwealth Trust [to RA]; the
1455 Canadian Institute for Advanced Research (CIFAR; grant RCZB/072 RG93193) [to DKM and
1456 EAS]; the Cambridge Biomedical Research Centre and NIHR Senior Investigator Awards
1457 and the British Oxygen Professorship of the Royal College of Anaesthetists [to DKM]; the
1458 Stephen Erskine Fellowship at Queens' College, Cambridge [to EAS]. BM is supported by
1459 the Natural Sciences and Engineering Research Council of Canada (NSERC Discovery
1460 Grant RGPIN #017-04265) and Canada Research Chairs Program. JYH is supported by the
1461 Helmholtz International BigBrain Analytics & Learning Laboratory, the Natural Sciences and
1462 Engineering Research Council of Canada, and Fonds de recherches de Québec. AMO is
1463 supported by the Canada Excellence Research Chairs program (215063); LN acknowledges
1464 support by the L'Oreal-Unesco for Women in Science Excellence Research Fellowship. LR
1465 acknowledges support of the Imperial College President's Scholarship. SLS is supported by
1466 funds from the Italian Department of Education [Fondo per gli Investimenti della Ricerca di
1467 Base (FIRB) 2003; Programmi di Ricerca di Rilevante Interesse nazionale (PRIN) 2008].
1468 RLC-H was supported by the Alex Mosley Charitable Trust and supporters of the Centre for
1469 Psychedelic Research during the period of data collection and now holds the Ralph Metzner
1470 Distinguished Professorship at UCSF. The original LSD study received support from a
1471 Crowd Funding Campaign and the Beckley Foundation, as part of the Beckley-Imperial
1472 Research Programme. The ketamine study was funded by the Bernard Wolfe Health
1473 Neuroscience Fund and the Wellcome Trust. Data acquisition for the sevoflurane dataset
1474 was funded by the Departments of Anesthesiology, Neurology, and Neuroradiology of the
1475 Klinikum rechts der Isar of the Technical University Munich. Computing infrastructure at the
1476 Wolfson Brain Imaging Centre (WBIC-HPHI) was funded by the MRC research infrastructure
1477 award (MR/M009041/1). We acknowledge the contribution of Santo Daime members for
1478 volunteering and for providing the Ayahuasca. We also thank members of the Cognition and
1479 Consciousness Imaging Group, and of the Network Neuroscience Lab, for many helpful
1480 discussions.

1481

1482 Conflicts of Interest

1483 RCH reports receiving scientific advisory fees in the last 2 years from: Enttheon Biomedical and
1484 Beckley Psytech. All other authors report no conflicts of interest.
1485

1486 Data availability

1487 Pharmacological-fMRI data are available upon request from the corresponding authors of
1488 the original publications referenced herein. The neurotransmitter receptor and transporter
1489 PET maps are available at https://github.com/netneurolab/hansen_receptors. The Allen
1490 Human Brain Atlas transcriptomic database is available at <https://human.brain-map.org/>;
1491 NeuroSynth is available at <https://github.com/neurosynth/neurosynth>. The ENIGMA toolbox
1492 is available at
1493 <https://github.com/MICA-MNI/ENIGMA>.

1494 References

- 1495
- 1496 1. Wandschneider, B. & Koepp, M. J. PharmacofMRI: Determining the functional
1497 anatomy of the effects of medication. *NeuroImage Clin.* **12**, 691–697 (2016).
 - 1498 2. Brown, E. N., Lydic, R. & Schiff, N. D. General Anesthesia, Sleep, and Coma. *N. Engl.*
1499 *J. Med.* **27**, 2638–50 (2010).
 - 1500 3. Cortese, S. *et al.* Comparative efficacy and tolerability of medications for attention-
1501 deficit hyperactivity disorder in children, adolescents, and adults: a systematic review
1502 and network meta-analysis. *Lancet Psychiatry* **5**, 727–738 (2018).
 - 1503 4. Faraone, S. V. The pharmacology of amphetamine and methylphenidate: Relevance to
1504 the neurobiology of attention-deficit/hyperactivity disorder and other psychiatric
1505 comorbidities. *Neurosci. Biobehav. Rev.* **87**, 255–270 (2018).
 - 1506 5. Moldofsky, H., Broughton, R. J. & Hill, J. D. A randomized trial of the long-term,
1507 continued efficacy and safety of modafinil in narcolepsy. *Sleep Med.* **1**, 109–116
1508 (2000).
 - 1509 6. Turner, D. C. *et al.* Cognitive enhancing effects of modafinil in healthy volunteers.
1510 *Psychopharmacology (Berl.)* **165**, 260–269 (2003).

- 1511 7. Minzenberg, M. J. & Carter, C. S. Modafinil: a review of neurochemical actions and
1512 effects on cognition. *Neuropsychopharmacol. Off. Publ. Am. Coll.*
1513 *Neuropsychopharmacol.* **33**, 1477–1502 (2008).
- 1514 8. Minzenberg, M. J., Watrous, A. J., Yoon, J. H., Ursu, S. & Carter, C. S. Modafinil shifts
1515 human locus coeruleus to low-tonic, high-phasic activity during functional MRI. *Science*
1516 **322**, 1700–1702 (2008).
- 1517 9. Kahbazi, M. *et al.* A randomized, double-blind and placebo-controlled trial of modafinil
1518 in children and adolescents with attention deficit and hyperactivity disorder. *Psychiatry*
1519 *Res.* **168**, 234–237 (2009).
- 1520 10. Manktelow, A. E., Menon, D. K., Sahakian, B. J. & Stamatakis, E. A. Working Memory
1521 after Traumatic Brain Injury: The Neural Basis of Improved Performance with
1522 Methylphenidate. *Front. Behav. Neurosci.* **11**, (2017).
- 1523 11. Storebø, O. J. *et al.* Methylphenidate for attention deficit hyperactivity disorder (ADHD)
1524 in children and adolescents – assessment of adverse events in non-randomised
1525 studies. *Cochrane Database Syst. Rev.* **2018**, CD012069 (2018).
- 1526 12. Carhart-Harris, R. *et al.* Trial of Psilocybin versus Escitalopram for Depression. *N. Engl.*
1527 *J. Med.* **384**, 1402–1411 (2021).
- 1528 13. de Gregorio, D. *et al.* Hallucinogens in mental health: Preclinical and clinical studies on
1529 LSD, psilocybin, MDMA, and ketamine. *J. Neurosci.* **41**, 891–900 (2021).
- 1530 14. Mitchell, J. M. *et al.* MDMA-assisted therapy for severe PTSD: a randomized, double-
1531 blind, placebo-controlled phase 3 study. *Nat. Med.* **2021 276 27**, 1025–1033 (2021).
- 1532 15. Davis, A. K. *et al.* Effects of Psilocybin-Assisted Therapy on Major Depressive Disorder:
1533 A Randomized Clinical Trial. *JAMA Psychiatry* (2020)
1534 doi:10.1001/jamapsychiatry.2020.3285.
- 1535 16. Vollenweider, F. X. & Preller, K. H. Psychedelic drugs: neurobiology and potential for
1536 treatment of psychiatric disorders. *Nat. Rev. Neurosci.* **21**, 611–624 (2020).
- 1537 17. Vargas, M. V., Meyer, R., Avanes, A. A., Rus, M. & Olson, D. E. Psychedelics and
1538 Other Psychoplastogens for Treating Mental Illness. *Front. Psychiatry* **12**, 1691 (2021).

- 1539 18. Luppi, A. I. *et al.* Consciousness-specific dynamic interactions of brain integration and
1540 functional diversity. *Nat. Commun.* **10**, (2019).
- 1541 19. Huang, Z., Zhang, J., Wu, J., Mashour, G. A. & Hudetz, A. G. Temporal circuit of
1542 macroscale dynamic brain activity supports human consciousness. *Sci. Adv.* **6**, 87–98
1543 (2020).
- 1544 20. Campbell, J. M. *et al.* Pharmacologically informed machine learning approach for
1545 identifying pathological states of unconsciousness via resting-state fMRI. *NeuroImage*
1546 **206**, 116316 (2020).
- 1547 21. Luppi, A. I. *et al.* Connectome Harmonic Decomposition of Human Brain Dynamics
1548 Reveals a Landscape of Consciousness. *bioRxiv* (2020)
1549 doi:10.1101/2020.08.10.244459.
- 1550 22. Sarasso, S. *et al.* Consciousness and complexity during unresponsiveness induced by
1551 propofol, xenon, and ketamine. *Curr. Biol.* **25**, 3099–3105 (2015).
- 1552 23. Schartner, M. M., Carhart-Harris, R. L., Barrett, A. B., Seth, A. K. &
1553 Muthukumaraswamy, S. D. Increased spontaneous MEG signal diversity for
1554 psychoactive doses of ketamine, LSD and psilocybin. *Sci. Rep.* **7**, 46421 (2017).
- 1555 24. Li, D. & Mashour, G. A. Cortical dynamics during psychedelic and anesthetized states
1556 induced by ketamine. *NeuroImage* **196**, 32–40 (2019).
- 1557 25. Johnson, M. W., Hendricks, P. S., Barrett, F. S. & Griffiths, R. R. Classic psychedelics:
1558 An integrative review of epidemiology, therapeutics, mystical experience, and brain
1559 network function. *Pharmacol. Ther.* **197**, 83–102 (2019).
- 1560 26. Carhart-Harris, R. L. & Goodwin, G. M. The Therapeutic Potential of Psychedelic
1561 Drugs: Past, Present, and Future. *Neuropsychopharmacol. Off. Publ. Am. Coll.*
1562 *Neuropsychopharmacol.* **42**, 2105–2113 (2017).
- 1563 27. Goulas, A. *et al.* The natural axis of transmitter receptor distribution in the human
1564 cerebral cortex. *Proc. Natl. Acad. Sci. U. S. A.* **118**, (2021).
- 1565 28. Zilles, K. & Palomero-Gallagher, N. Multiple transmitter receptors in regions and layers
1566 of the human cerebral cortex. *Front. Neuroanat.* **11**, 78 (2017).

- 1567 29. Suárez, L. E., Markello, R. D., Betzel, R. F. & Misic, B. Linking Structure and Function
1568 in Macroscale Brain Networks. *Trends Cogn. Sci.* **24**, 302–315 (2020).
- 1569 30. Shine, J. M. Neuromodulatory Influences on Integration and Segregation in the Brain.
1570 *Trends Cogn. Sci.* **23**, 572–583 (2019).
- 1571 31. Hansen, J. Y. *et al.* Mapping neurotransmitter systems to the structural and functional
1572 organization of the human neocortex. *Nat. Neurosci.* **(accepted)**, 1–26 (2022).
- 1573 32. Trapani, G., Altomare, C., Sanna, E., Biggio, G. & Liso, G. Propofol in Anesthesia.
1574 Mechanism of Action, Structure-Activity Relationships, and Drug Delivery. *Curr. Med.*
1575 *Chem.* **7**, 249–271 (2000).
- 1576 33. Jurd, R. *et al.* General anesthetic actions *in vivo* strongly attenuated by a point mutation
1577 in the GABA_A receptor β 3 subunit. *FASEB J.* **17**, 250–252 (2003).
- 1578 34. Yip, G. M. S. *et al.* A propofol binding site on mammalian GABA_A receptors identified
1579 by photolabeling. *Nat. Chem. Biol.* **9**, 715–720 (2013).
- 1580 35. Nishikawa, K. & Harrison, N. L. The Actions of Sevoflurane and Desflurane on the γ -
1581 Aminobutyric Acid Receptor Type A: Effects of TM2 Mutations in the α and β Subunits.
1582 *Anesthesiology* **99**, 678–684 (2003).
- 1583 36. Wu, J., Harata, N. & Akaike, N. Potentiation by sevoflurane of the gamma-aminobutyric
1584 acid-induced chloride current in acutely dissociated CA1 pyramidal neurones from rat
1585 hippocampus. *Br. J. Pharmacol.* **119**, 1013–1021 (1996).
- 1586 37. Hirota, K. & Roth, S. H. Sevoflurane modulates both GABAA and GABAB receptors in
1587 area CA1 of rat hippocampus. *Br. J. Anaesth.* **78**, 60–65 (1997).
- 1588 38. Jenkins, A., Franks, N. P. & Lieb, W. R. Effects of temperature and volatile anesthetics
1589 on GABA(A) receptors. *Anesthesiology* **90**, 484–491 (1999).
- 1590 39. Campagna, J. A., Miller, K. W. & Forman, S. A. Mechanisms of actions of inhaled
1591 anesthetics. *N. Engl. J. Med.* **348**, 2110–2124 (2003).
- 1592 40. Domino, E. F. Taming the ketamine tiger. *Anesthesiology* **113**, 678–684 (2010).
- 1593 41. Domino, E. F., Chodoff, P. & Corssen, G. Pharmacologic effects of CI-581, a new
1594 dissociative anesthetic, in man. *Clin. Pharmacol. Ther.* **6**, 279–291 (1965).

- 1595 42. Krystal, J. H. *et al.* Subanesthetic Effects of the Noncompetitive NMDA Antagonist,
1596 Ketamine, in Humans: Psychotomimetic, Perceptual, Cognitive, and Neuroendocrine
1597 Responses. *Arch. Gen. Psychiatry* **51**, 199–214 (1994).
- 1598 43. Mashour, G. A. Top-down mechanisms of anesthetic-induced unconsciousness. *Front.*
1599 *Syst. Neurosci.* **8**, (2014).
- 1600 44. Olney, J. W., Newcomer, J. W. & Farber, N. B. NMDA receptor hypofunction model of
1601 schizophrenia. *J. Psychiatr. Res.* **33**, 523–533 (1999).
- 1602 45. Li, L. & Vlisides, P. E. Ketamine: 50 Years of Modulating the Mind. *Front. Hum.*
1603 *Neurosci.* **10**, (2016).
- 1604 46. Nichols, D. E. Psychedelics. *Pharmacol. Rev.* **68**, 264–355 (2016).
- 1605 47. Glennon, R. A., Titeler, M. & McKenney, J. D. Evidence for 5-HT₂ involvement in the
1606 mechanism of action of hallucinogenic agents. *Life Sci.* **35**, 2505–2511 (1984).
- 1607 48. Nichols, D. E. Dark Classics in Chemical Neuroscience: Lysergic Acid Diethylamide
1608 (LSD). *ACS Chem. Neurosci.* **9**, 2331–2343 (2018).
- 1609 49. Nichols, D. E. Hallucinogens. *Pharmacol. Ther.* **101**, 131–181 (2004).
- 1610 50. Sleight, J., Harvey, M., Voss, L. & Denny, B. Ketamine – More mechanisms of action
1611 than just NMDA blockade. *Trends Anaesth. Crit. Care* **4**, 76–81 (2014).
- 1612 51. Spindler, L. R. B. *et al.* Dopaminergic brainstem disconnection is common to
1613 pharmacological and pathological consciousness perturbation. *Proc. Natl. Acad. Sci. U.*
1614 *S. A.* **118**, e2026289118 (2021).
- 1615 52. Lawn, T. *et al.* Differential contributions of serotonergic and dopaminergic functional
1616 connectivity to the phenomenology of LSD. *Psychopharmacology (Berl.)* (2022)
1617 doi:10.1007/S00213-022-06117-5.
- 1618 53. Ballentine, G., Friedman, S. F. & Bzdok, D. Trips and neurotransmitters: Discovering
1619 principled patterns across 6850 hallucinogenic experiences. *Sci. Adv.* **8**, eabl6989
1620 (2022).

- 1621 54. Sydnor, V. J. *et al.* Neurodevelopment of the association cortices: Patterns,
1622 mechanisms, and implications for psychopathology. *Neuron* (2021)
1623 doi:10.1016/j.neuron.2021.06.016.
- 1624 55. Huntenburg, J. M. *et al.* A Systematic Relationship Between Functional Connectivity
1625 and Intracortical Myelin in the Human Cerebral Cortex. *Cereb. Cortex* **27**, 981–997
1626 (2017).
- 1627 56. Valk, S. L. *et al.* Genetic and phylogenetic uncoupling of structure and function in
1628 human transmodal cortex. *bioRxiv* **5**, 2021.06.08.447522 (2021).
- 1629 57. Margulies, D. S. *et al.* Situating the default-mode network along a principal gradient of
1630 macroscale cortical organization. *Proc. Natl. Acad. Sci. U. S. A.* **113**, 12574–12579
1631 (2016).
- 1632 58. Burt, J. B. *et al.* Hierarchy of transcriptomic specialization across human cortex
1633 captured by structural neuroimaging topography. *Nat. Neurosci.* **21**, 1251–1259 (2018).
- 1634 59. Hansen, J. Y. *et al.* Mapping gene transcription and neurocognition across human
1635 neocortex. *Nat. Hum. Behav.* 1–11 (2021) doi:10.1038/s41562-021-01082-z.
- 1636 60. Carhart-Harris, R. L. *et al.* Neural correlates of the LSD experience revealed by
1637 multimodal neuroimaging. *Proc. Natl. Acad. Sci.* **113**, 201518377 (2016).
- 1638 61. Carhart-Harris, R. L. *et al.* Neural correlates of the psychedelic state as determined by
1639 fMRI studies with psilocybin. *Proc. Natl. Acad. Sci.* **109**, 2138–2143 (2012).
- 1640 62. Viol, A., Palhano-Fontes, F., Onias, H., De Araujo, D. B. & Viswanathan, G. M.
1641 Shannon entropy of brain functional complex networks under the influence of the
1642 psychedelic Ayahuasca. *Sci. Rep.* **7**, (2017).
- 1643 63. Dandash, O. *et al.* Selective Augmentation of Striatal Functional Connectivity Following
1644 NMDA Receptor Antagonism: Implications for Psychosis. *Neuropsychopharmacology*
1645 **40**, 622–631 (2015).
- 1646 64. Esposito, R. *et al.* Acute Effects of Modafinil on Brain Resting State Networks in Young
1647 Healthy Subjects. *PLoS ONE* **8**, (2013).

- 1648 65. Ranft, A. *et al.* Neural Correlates of Sevoflurane-induced Unconsciousness Identified
1649 by Simultaneous Functional Magnetic Resonance Imaging and
1650 Electroencephalography. *Anesthesiology* **125**, 861–872 (2016).
- 1651 66. Stamatakis, E. A., Adapa, R. M., Absalom, A. R. & Menon, D. K. Changes in resting
1652 neural connectivity during propofol sedation. *PloS One* **5**, e14224 (2010).
- 1653 67. Naci, L., Sinai, L. & Owen, A. M. Detecting and interpreting conscious experiences in
1654 behaviorally non-responsive patients. *NeuroImage* **145**, 304–313 (2017).
- 1655 68. Dipasquale, O. *et al.* Unravelling the effects of methylphenidate on the dopaminergic
1656 and noradrenergic functional circuits. doi:10.1038/s41386-020-0724-x.
- 1657 69. Dipasquale, O. *et al.* Receptor-Enriched Analysis of functional connectivity by targets
1658 (REACT): A novel, multimodal analytical approach informed by PET to study the
1659 pharmacodynamic response of the brain under MDMA. (2019)
1660 doi:10.1016/j.neuroimage.2019.04.007.
- 1661 70. Kringelbach, M. L. *et al.* Dynamic coupling of whole-brain neuronal and
1662 neurotransmitter systems. *Proc. Natl. Acad. Sci. U. S. A.* **117**, 9566–9576 (2020).
- 1663 71. Deco, G. *et al.* Whole-Brain Multimodal Neuroimaging Model Using Serotonin Receptor
1664 Maps Explains Non-linear Functional Effects of LSD. *Curr. Biol.* **28**, 3065–3074 (2018).
- 1665 72. Burt, J. *et al.* Transcriptomics-informed large-scale cortical model captures topography
1666 of pharmacological neuroimaging effects of LSD. *eLife* **10**, (2021).
- 1667 73. Parker Singleton, S. A. *et al.* Psychedelics Flatten the brain's energy landscape:
1668 evidence from receptor-informed network control theory. *bioRxiv* 2021.05.14.444193
1669 (2021) doi:10.1101/2021.05.14.444193.
- 1670 74. Kaller, S. *et al.* Test–retest measurements of dopamine D1-type receptors using
1671 simultaneous PET/MRI imaging. *Eur. J. Nucl. Med. Mol. Imaging* **44**, (2017).
- 1672 75. Sandiego, C. M. *et al.* Reference region modeling approaches for amphetamine
1673 challenge studies with [¹¹C]FLB 457 and PET. *J. Cereb. Blood Flow Metab. Off. J. Int.*
1674 *Soc. Cereb. Blood Flow Metab.* **35**, 623–629 (2015).

- 1675 76. Slifstein, M. *et al.* Deficits in prefrontal cortical and extrastriatal dopamine release in
1676 schizophrenia: a positron emission tomographic functional magnetic resonance imaging
1677 study. *JAMA Psychiatry* **72**, 316–324 (2015).
- 1678 77. Smith, C. T. *et al.* Partial-volume correction increases estimated dopamine D2-like
1679 receptor binding potential and reduces adult age differences. *J. Cereb. Blood Flow*
1680 *Metab. Off. J. Int. Soc. Cereb. Blood Flow Metab.* **39**, 822–833 (2019).
- 1681 78. Zakiniaez, Y. *et al.* Sex differences in amphetamine-induced dopamine release in the
1682 dorsolateral prefrontal cortex of tobacco smokers. *Neuropsychopharmacol. Off. Publ.*
1683 *Am. Coll. Neuropsychopharmacol.* **44**, 2205–2211 (2019).
- 1684 79. Dukart, J. *et al.* Cerebral blood flow predicts differential neurotransmitter activity. *Sci.*
1685 *Rep.* **8**, 4074 (2018).
- 1686 80. Sanchez-Rangel, E. *et al.* Norepinephrine transporter availability in brown fat is
1687 reduced in obesity: a human PET study with [11C] MRB. *Int. J. Obes.* **44**, 964–967
1688 (2020).
- 1689 81. Ding, Y.-S. *et al.* PET imaging of the effects of age and cocaine on the norepinephrine
1690 transporter in the human brain using (S,S)-[(11)C]O-methylreboxetine and HRRT.
1691 *Synap. N. Y. N* **64**, 30–38 (2010).
- 1692 82. Belfort-DeAguiar, R. *et al.* Noradrenergic Activity in the Human Brain: A Mechanism
1693 Supporting the Defense Against Hypoglycemia. *J. Clin. Endocrinol. Metab.* **103**, 2244–
1694 2252 (2018).
- 1695 83. Li, C. R. *et al.* Decreased norepinephrine transporter availability in obesity: Positron
1696 Emission Tomography imaging with (S,S)-[(11)C]O-methylreboxetine. *NeuroImage* **86**,
1697 306–310 (2014).
- 1698 84. Savli, M. *et al.* Normative database of the serotonergic system in healthy subjects using
1699 multi-tracer PET. *NeuroImage* **63**, 447–459 (2012).
- 1700 85. Gallezot, J.-D. *et al.* Kinetic modeling of the serotonin 5-HT(1B) receptor radioligand
1701 [(11)C]P943 in humans. *J. Cereb. Blood Flow Metab. Off. J. Int. Soc. Cereb. Blood*
1702 *Flow Metab.* **30**, 196–210 (2010).

- 1703 86. Matuskey, D. *et al.* Reductions in brain 5-HT_{1B} receptor availability in primarily
1704 cocaine-dependent humans. *Biol. Psychiatry* **76**, 816–822 (2014).
- 1705 87. Murrough, J. W. *et al.* The effect of early trauma exposure on serotonin type 1B
1706 receptor expression revealed by reduced selective radioligand binding. *Arch. Gen.*
1707 *Psychiatry* **68**, 892–900 (2011).
- 1708 88. Pittenger, C. *et al.* OCD is associated with an altered association between sensorimotor
1709 gating and cortical and subcortical 5-HT_{1b} receptor binding. *J. Affect. Disord.* **196**, 87–
1710 96 (2016).
- 1711 89. Saricicek, A. *et al.* Test-retest reliability of the novel 5-HT_{1B} receptor PET radioligand
1712 [¹¹C]P943. *Eur. J. Nucl. Med. Mol. Imaging* **42**, 468–477 (2015).
- 1713 90. Beliveau, V. *et al.* A High-Resolution In Vivo Atlas of the Human Brain’s Serotonin
1714 System. *J. Neurosci.* **37**, 120 (2017).
- 1715 91. Radhakrishnan, R. *et al.* In vivo 5-HT₆ and 5-HT_{2A} receptor availability in antipsychotic
1716 treated schizophrenia patients vs. unmedicated healthy humans measured with
1717 [¹¹C]GSK215083 PET. *Psychiatry Res. Neuroimaging* **295**, 111007 (2020).
- 1718 92. Radhakrishnan, R. *et al.* Age-Related Change in 5-HT₆ Receptor Availability in Healthy
1719 Male Volunteers Measured with ¹¹C-GSK215083 PET. *J. Nucl. Med.* **59**, 1445–1450
1720 (2018).
- 1721 93. Hillmer, A. T. *et al.* Imaging of cerebral $\alpha 4\beta 2^*$ nicotinic acetylcholine receptors with (-)-
1722 [(¹⁸F)]Flubatine PET: Implementation of bolus plus constant infusion and sensitivity to
1723 acetylcholine in human brain. *NeuroImage* **141**, 71–80 (2016).
- 1724 94. Baldassarri, S. R. *et al.* Use of Electronic Cigarettes Leads to Significant Beta₂-
1725 Nicotinic Acetylcholine Receptor Occupancy: Evidence From a PET Imaging Study.
1726 *Nicotine Tob. Res. Off. J. Soc. Res. Nicotine Tob.* **20**, 425–433 (2018).
- 1727 95. Naganawa, M. *et al.* First-in-Human Assessment of ¹¹C-LSN3172176, an M₁
1728 Muscarinic Acetylcholine Receptor PET Radiotracer. *J. Nucl. Med. Off. Publ. Soc. Nucl.*
1729 *Med.* **62**, 553–560 (2021).

- 1730 96. Bedard, M.-A. *et al.* Brain cholinergic alterations in idiopathic REM sleep behaviour
1731 disorder: a PET imaging study with 18F-FEOBV. *Sleep Med.* **58**, 35–41 (2019).
- 1732 97. Aghourian, M. *et al.* Quantification of brain cholinergic denervation in Alzheimer's
1733 disease using PET imaging with [18F]-FEOBV. *Mol. Psychiatry* **22**, 1531–1538 (2017).
- 1734 98. Smart, K. *et al.* Sex differences in [11C]ABP688 binding: a positron emission
1735 tomography study of mGlu5 receptors. *Eur. J. Nucl. Med. Mol. Imaging* **46**, 1179–1183
1736 (2019).
- 1737 99. DuBois, J. M. *et al.* Characterization of age/sex and the regional distribution of mGluR5
1738 availability in the healthy human brain measured by high-resolution [(11)C]ABP688
1739 PET. *Eur. J. Nucl. Med. Mol. Imaging* **43**, 152–162 (2016).
- 1740 100. Nørgaard, M. *et al.* A High-Resolution In Vivo Atlas of the Human Brain's
1741 Benzodiazepine Binding Site of GABA A Receptors. *NeuroImage* **232**, 117878 (2021).
- 1742 101. Gallezot, J.-D. *et al.* Determination of receptor occupancy in the presence of mass
1743 dose: [11C]GSK189254 PET imaging of histamine H3 receptor occupancy by PF-
1744 03654746. *J. Cereb. Blood Flow Metab. Off. J. Int. Soc. Cereb. Blood Flow Metab.* **37**,
1745 1095–1107 (2017).
- 1746 102. D'Souza, D. C. *et al.* Rapid Changes in CB1 Receptor Availability in Cannabis
1747 Dependent Males after Abstinence from Cannabis. *Biol. Psychiatry Cogn. Neurosci.*
1748 *Neuroimaging* **1**, 60–67 (2016).
- 1749 103. Neumeister, A. *et al.* Positron emission tomography shows elevated cannabinoid CB1
1750 receptor binding in men with alcohol dependence. *Alcohol. Clin. Exp. Res.* **36**, 2104–
1751 2109 (2012).
- 1752 104. Normandin, M. D. *et al.* Imaging the cannabinoid CB1 receptor in humans with
1753 [11C]OMAR: assessment of kinetic analysis methods, test-retest reproducibility, and
1754 gender differences. *J. Cereb. Blood Flow Metab. Off. J. Int. Soc. Cereb. Blood Flow*
1755 *Metab.* **35**, 1313–1322 (2015).
- 1756 105. Ranganathan, M. *et al.* Reduced Brain Cannabinoid Receptor Availability in
1757 Schizophrenia. *Biol. Psychiatry* **79**, 997–1005 (2016).

- 1758 106. Kantonen, T. *et al.* Interindividual variability and lateralization of μ -opioid receptors in
1759 the human brain. *NeuroImage* **217**, 116922 (2020).
- 1760 107. Schaefer, A. *et al.* Local-Global Parcellation of the Human Cerebral Cortex from
1761 Intrinsic Functional Connectivity MRI. *Cereb. Cortex* **28**, 3095–3114 (2018).
- 1762 108. Cammoun, L. *et al.* Mapping the human connectome at multiple scales with diffusion
1763 spectrum MRI. *J. Neurosci. Methods* **203**, 386–397 (2012).
- 1764 109. Hansen, J. Y. *et al.* Molecular and connectomic vulnerability shape cross-disorder
1765 cortical abnormalities. *bioRxiv* 2022.01.21.476409 (2022)
1766 doi:10.1101/2022.01.21.476409.
- 1767 110. Betzel, R. F. & Bassett, D. S. Specificity and robustness of long-distance connections in
1768 weighted, interareal connectomes. *Proc Natl Acad Sci USA* (2018)
1769 doi:10.1073/pnas.1720186115.
- 1770 111. Roberts, J. A. *et al.* The contribution of geometry to the human connectome.
1771 *NeuroImage* **124**, 379–393 (2016).
- 1772 112. Stiso, J. & Bassett, D. S. Spatial Embedding Imposes Constraints on Neuronal Network
1773 Architectures. *Trends Cogn. Sci.* **22**, 1127–1142 (2018).
- 1774 113. Wold, S., Josefson, M., Gottfries, J. & Linusson, A. The utility of multivariate design in
1775 PLS modeling. *J. Chemom.* **18**, 156–165 (2004).
- 1776 114. McIntosh, A. R. & Lobaugh, N. J. Partial least squares analysis of neuroimaging data:
1777 applications and advances. *NeuroImage* **23 Suppl 1**, S250-263 (2004).
- 1778 115. Krishnan, A., Williams, L. J., McIntosh, A. R. & Abdi, H. Partial Least Squares (PLS)
1779 methods for neuroimaging: A tutorial and review. *NeuroImage* **56**, 455–475 (2011).
- 1780 116. McIntosh, A. R. & Mišić, B. Multivariate Statistical Analyses for Neuroimaging Data.
1781 *Annu. Rev. Psychol.* **64**, 499–525 (2013).
- 1782 117. Markello, R. D. & Misic, B. Comparing spatial null models for brain maps. *NeuroImage*
1783 **236**, 118052 (2021).
- 1784 118. Váša, F. & Mišić, B. M. *Null Models in Network Neuroscience*.

- 1785 119. Váša, F. *et al.* Adolescent tuning of association cortex in human structural brain
1786 networks. *Cereb. Cortex* **28**, 281–294 (2018).
- 1787 120. Alexander-Bloch, A. F. *et al.* On testing for spatial correspondence between maps of
1788 human brain structure and function. *NeuroImage* **178**, 540–551 (2018).
- 1789 121. Yeo, B. T. T. *et al.* The organization of the human cerebral cortex estimated by intrinsic
1790 functional connectivity. *J. Neurophysiol.* **106**, 1125–1165 (2011).
- 1791 122. Hill, J. *et al.* Similar patterns of cortical expansion during human development and
1792 evolution. *Proc. Natl. Acad. Sci.* **107**, 13135–13140 (2010).
- 1793 123. Hawrylycz, M. J. *et al.* An anatomically comprehensive atlas of the adult human brain
1794 transcriptome. *Nature* **489**, 391–399 (2012).
- 1795 124. Yarkoni, T., Poldrack, R. A., Nichols, T. E., Van Essen, D. C. & Wager, T. D. Large-
1796 scale automated synthesis of human functional neuroimaging data. *Nat. Methods* **8**,
1797 665–670 (2011).
- 1798 125. Luppi, A. I. *et al.* A synergistic core for human brain evolution and cognition. *Nat.*
1799 *Neurosci.* **25**, 771–782 (2022).
- 1800 126. Larivière, S. *et al.* The ENIGMA Toolbox: multiscale neural contextualization of multisite
1801 neuroimaging datasets. *Nat. Methods* **2021 187 18**, 698–700 (2021).
- 1802 127. Sun, D. *et al.* Large-scale mapping of cortical alterations in 22q11.2 deletion syndrome:
1803 Convergence with idiopathic psychosis and effects of deletion size. *Mol. Psychiatry* **25**,
1804 1822–1834 (2020).
- 1805 128. Hoogman, M. *et al.* Brain Imaging of the Cortex in ADHD: A Coordinated Analysis of
1806 Large-Scale Clinical and Population-Based Samples. *Am. J. Psychiatry* **176**, 531–542
1807 (2019).
- 1808 129. van Rooij, D. *et al.* Cortical and Subcortical Brain Morphometry Differences Between
1809 Patients With Autism Spectrum Disorder and Healthy Individuals Across the Lifespan:
1810 Results From the ENIGMA ASD Working Group. *Am. J. Psychiatry* **175**, 359–369
1811 (2018).

- 1812 130. Whelan, C. D. *et al.* Structural brain abnormalities in the common epilepsies assessed
1813 in a worldwide ENIGMA study. *Brain J. Neurol.* **141**, 391–408 (2018).
- 1814 131. Schmaal, L. *et al.* Cortical abnormalities in adults and adolescents with major
1815 depression based on brain scans from 20 cohorts worldwide in the ENIGMA Major
1816 Depressive Disorder Working Group. *Mol. Psychiatry* **22**, 900–909 (2017).
- 1817 132. Boedhoe, P. S. W. *et al.* Cortical Abnormalities Associated With Pediatric and Adult
1818 Obsessive-Compulsive Disorder: Findings From the ENIGMA Obsessive-Compulsive
1819 Disorder Working Group. *Am. J. Psychiatry* **175**, 453–462 (2018).
- 1820 133. van Erp, T. G. M. *et al.* Cortical Brain Abnormalities in 4474 Individuals With
1821 Schizophrenia and 5098 Control Subjects via the Enhancing Neuro Imaging Genetics
1822 Through Meta Analysis (ENIGMA) Consortium. *Biol. Psychiatry* **84**, 644–654 (2018).
- 1823 134. Hibar, D. P. *et al.* Cortical abnormalities in bipolar disorder: an MRI analysis of 6503
1824 individuals from the ENIGMA Bipolar Disorder Working Group. *Mol. Psychiatry* **23**,
1825 932–942 (2018).
- 1826 135. Laansma, M. A. *et al.* International Multicenter Analysis of Brain Structure Across
1827 Clinical Stages of Parkinson’s Disease. *Mov. Disord.* **36**, 2583–2594 (2021).
- 1828 136. Paquola, C. *et al.* A multi-scale cortical wiring space links cellular architecture and
1829 functional dynamics in the human brain. *PLOS Biol.* **18**, e3000979 (2020).
- 1830 137. Viol, A. *et al.* Characterizing complex networks using entropy-degree diagrams:
1831 Unveiling changes in functional brain connectivity induced by Ayahuasca. *Entropy* **21**,
1832 (2019).
- 1833 138. Luppi, A. I. *et al.* LSD alters dynamic integration and segregation in the human brain.
1834 *NeuroImage* **227**, 117653 (2021).
- 1835 139. Atasoy, S. *et al.* Connectome-harmonic decomposition of human brain activity reveals
1836 dynamical repertoire re-organization under LSD. *Sci. Rep.* **7**, 1–18 (2017).
- 1837 140. Lord, L. D. *et al.* Dynamical exploration of the repertoire of brain networks at rest is
1838 modulated by psilocybin. *NeuroImage* **199**, 127–142 (2019).

- 1839 141. Schartner, M. *et al.* Complexity of multi-dimensional spontaneous EEG decreases
1840 during propofol induced general anaesthesia. *PLoS ONE* **10**, (2015).
- 1841 142. Toker, D. *et al.* Consciousness is supported by near-critical cortical electrodynamics.
1842 doi:10.1073/pnas.XXXXXXXXXX.
- 1843 143. Carhart-Harris, R. L. & Friston, K. J. REBUS and the anarchic brain: Toward a unified
1844 model of the brain action of psychedelics. *Pharmacol. Rev.* **71**, 316–344 (2019).
- 1845 144. Varley, T. F. *et al.* Consciousness & Brain Functional Complexity in Propofol
1846 Anaesthesia. *Sci. Rep.* **10**, 1–13 (2020).
- 1847 145. Varley, T. F. *et al.* Fractal dimension of cortical functional connectivity networks &
1848 severity of disorders of consciousness. *PLoS ONE* **15**, 1–20 (2020).
- 1849 146. Varley, T. F., Carhart-Harris, R., Roseman, L., Menon, D. K. & Stamatakis, E. A.
1850 Serotonergic psychedelics LSD & psilocybin increase the fractal dimension of cortical
1851 brain activity in spatial and temporal domains. *NeuroImage* **220**, (2020).
- 1852 147. Lebedev, A. V. *et al.* LSD-induced entropic brain activity predicts subsequent
1853 personality change. *Hum. Brain Mapp.* **37**, 3203–3213 (2016).
- 1854 148. Bonhomme, V. *et al.* Resting-state Network-specific Breakdown of Functional
1855 Connectivity during Ketamine Alteration of Consciousness in Volunteers.
1856 *Anesthesiology* **125**, 873–888 (2016).
- 1857 149. Boveroux, P., Vanhaudenhuyse, A. & Phillips, C. Breakdown of within- and between-
1858 network Resting State during Propofol-induced Loss of Consciousness. *Anesthesiology*
1859 **113**, 1038–1053 (2010).
- 1860 150. Wu, H. *et al.* Anterior precuneus related to the recovery of consciousness. *NeuroImage*
1861 *Clin.* **33**, 102951 (2022).
- 1862 151. Palhano-Fontes, F. *et al.* The psychedelic state induced by Ayahuasca modulates the
1863 activity and connectivity of the Default Mode Network. *PLoS ONE* **10**, (2015).
- 1864 152. Girn, M. *et al.* LSD flattens the functional hierarchy of the human brain. *bioRxiv*
1865 2020.05.01.072314 (2020) doi:10.1101/2020.05.01.072314.

- 1866 153. Demirtaş, M. *et al.* Hierarchical Heterogeneity across Human Cortex Shapes Large-
1867 Scale Neural Dynamics. *Neuron* **101**, 1181-1194.e13 (2019).
- 1868 154. Beul, S. F. & Hilgetag, C. C. Neuron density fundamentally relates to architecture and
1869 connectivity of the primate cerebral cortex. *NeuroImage* **189**, 777–792 (2019).
- 1870 155. Baum, G. L. *et al.* Development of structure–function coupling in human brain networks
1871 during youth. *Proc. Natl. Acad. Sci. U. S. A.* **117**, 771–778 (2020).
- 1872 156. Alamia, A., Timmermann, C., Vanrullen, R. & Carhart-Harris, R. L. DMT alters cortical
1873 travelling waves. *eLife* **9**, 1–16 (2020).
- 1874 157. Lawrence, D. W., Carhart-Harris, R., Griffiths, R. & Timmermann, C. Phenomenology
1875 and content of the inhaled N, N-dimethyltryptamine (N, N-DMT) experience. *Sci. Rep.*
1876 **12**, 8562 (2022).
- 1877 158. Doss, M. K. *et al.* The Acute Effects of the Atypical Dissociative Hallucinogen Salvinorin
1878 A on Functional Connectivity in the Human Brain. *Sci. Rep.* **10**, 16392 (123AD).
- 1879 159. Akeju, O. *et al.* Disruption of thalamic functional connectivity is a neural correlate of
1880 dexmedetomidine-induced unconsciousness. *eLife* **3**, (2014).
- 1881 160. Guldenmund, P. *et al.* Brain functional connectivity differentiates dexmedetomidine
1882 from propofol and natural sleep. *BJA Br. J. Anaesth.* **119**, 674–684 (2017).
- 1883 161. Nelson, L. E. *et al.* The α 2-adrenoceptor agonist dexmedetomidine converges on an
1884 endogenous sleep-promoting pathway to exert its sedative effects. *Anesthesiology* **98**,
1885 428–436 (2003).
- 1886 162. Lee, U. *et al.* Disruption of frontal-parietal communication by ketamine, propofol, and
1887 sevoflurane. *Anesthesiology* **118**, 1264–75 (2013).
- 1888 163. Van de Bittner, G. C., Ricq, E. L. & Hooker, J. M. A philosophy for CNS radiotracer
1889 design. *Acc. Chem. Res.* **47**, 3127–3134 (2014).
- 1890 164. Elsinga, P. H., Hatano, K. & Ishiwata, K. PET tracers for imaging of the dopaminergic
1891 system. *Curr. Med. Chem.* **13**, 2139–2153 (2006).
- 1892 165. Redinbaugh, M. J. *et al.* Thalamus modulates consciousness via layer-specific control
1893 of cortex. *Neuron* **106**, 66-75.e12 (2020).

- 1894 166. Tasserie, J. *et al.* Deep brain stimulation of the thalamus restores signatures of
1895 consciousness in a nonhuman primate model. *Sci Adv* **8**, 5547 (2022).
- 1896 167. Barttfeld, P. *et al.* Factoring the brain signatures of anesthesia concentration and level
1897 of arousal across individuals. *NeuroImage Clin.* **9**, 385–391 (2015).
- 1898 168. Preller, K. H. *et al.* Changes in global and thalamic brain connectivity in LSD-induced
1899 altered states of consciousness are attributable to the 5-HT_{2A} receptor. *eLife* **7**, (2018).
- 1900 169. Preller, K. H. *et al.* Effective connectivity changes in LSD-induced altered states of
1901 consciousness in humans. *Proc. Natl. Acad. Sci. U. S. A.* **116**, 2743–2748 (2019).
- 1902 170. Shine, J. M. The thalamus integrates the macrosystems of the brain to facilitate
1903 complex, adaptive brain network dynamics. *Prog. Neurobiol.* 101951 (2020)
1904 doi:10.1016/j.pneurobio.2020.101951.
- 1905 171. Kringelbach, M. L. & Deco, G. Brain States and Transitions: Insights from
1906 Computational Neuroscience. *Cell Rep.* **32**, 108128 (2020).
- 1907 172. Cofré, R. *et al.* Whole-brain models to explore altered states of consciousness from the
1908 bottom up. *Brain Sci.* **10**, 1–29 (2020).
- 1909 173. Deco, G. & Kringelbach, M. L. Great expectations: Using whole-brain computational
1910 connectomics for understanding neuropsychiatric disorders. *Neuron* **84**, 892–905
1911 (2014).
- 1912 174. Shine, J. M. *et al.* Computational models link cellular mechanisms of neuromodulation
1913 to large-scale neural dynamics. *Nat. Neurosci.* 1–12 (2021) doi:10.1038/s41593-021-
1914 00824-6.
- 1915 175. Herzog, R. *et al.* A mechanistic model of the neural entropy increase elicited by
1916 psychedelic drugs. *Sci. Rep.* **10**, 17725 (2020).
- 1917 176. Luppi, A. I. *et al.* Whole-brain modelling identifies distinct but convergent paths to
1918 unconsciousness in anaesthesia and disorders of consciousness. *Commun. Biol.* **5**,
1919 384 (2022).

- 1920 177. Tian, Y., Margulies, D., Breakspear, M. & Zalesky, A. Topographic organization of the
1921 human subcortex unveiled with functional connectivity gradients. *Nat. Neurosci.* **23**,
1922 1421–1432 (2020).
- 1923 178. Veselis, R. A., Feshchenko, V. A., Reinsel, R. A., Beattie, B. & Akhurst, T. J. Propofol
1924 and thiopental do not interfere with regional cerebral blood flow response at sedative
1925 concentrations. *Anesthesiology* **102**, 26–34 (2005).
- 1926 179. Johnston, A. J. *et al.* Effects of propofol on cerebral oxygenation and metabolism after
1927 head injury. *Br. J. Anaesth.* **91**, 781–786 (2003).
- 1928 180. Hemmings, H. C. *et al.* Emerging molecular mechanisms of general anesthetic action.
1929 *Trends Pharmacol. Sci.* **26**, 503–510 (2005).
- 1930 181. Bademosi, A. T. *et al.* Trapping of Syntaxin1a in Presynaptic Nanoclusters by a
1931 Clinically Relevant General Anesthetic. *Cell Rep.* **22**, 427–440 (2018).
- 1932 182. Wang, Y. *et al.* Effects of propofol on the dopamine, metabolites and GABAA receptors
1933 in media prefrontal cortex in freely moving rats. *Am J Transl Res* vol. 8 2301–2308
1934 www.ajtr.org/ISSN:1943-8141/AJTR0024580 (2016).
- 1935 183. Guo, J. *et al.* Dopamine transporter in the ventral tegmental area modulates recovery
1936 from propofol anesthesia in rats. *J. Chem. Neuroanat.* **121**, 102083 (2022).
- 1937 184. Naci, L. *et al.* Functional diversity of brain networks supports consciousness and verbal
1938 intelligence. *Sci. Rep.* **8**, 1–15 (2018).
- 1939 185. Coppola, P. *et al.* Network dynamics scale with levels of awareness. *NeuroImage*
1940 119128 (2022) doi:10.1016/J.NEUROIMAGE.2022.119128.
- 1941 186. Kandeepan, S. *et al.* Modeling an auditory stimulated brain under altered states of
1942 consciousness using the generalized ising model. *NeuroImage* **223**, 117367 (2020).
- 1943 187. Solt, K., Eger, E. I. & Raines, D. E. Differential modulation of human N-methyl-D-
1944 aspartate receptors by structurally diverse general anesthetics. *Anesth. Analg.* **102**,
1945 1407–1411 (2006).

- 1946 188. Hollmann, M. W., Liu, H. T., Hoenemann, C. W., Liu, W. H. & Durieux, M. E. Modulation
1947 of NMDA receptor function by ketamine and magnesium. Part II: interactions with
1948 volatile anesthetics. *Anesth. Analg.* **92**, 1182–1191 (2001).
- 1949 189. Scheller, M., Bufler, J., Schneck, H., Kochs, E. & Franke, C. Isoflurane and sevoflurane
1950 interact with the nicotinic acetylcholine receptor channels in micromolar concentrations.
1951 *Anesthesiology* **86**, 118–127 (1997).
- 1952 190. Alkire, M. T., McReynolds, J. R., Hahn, E. L. & Trivedi, A. N. Thalamic microinjection of
1953 nicotine reverses sevoflurane-induced loss of righting reflex in the rat. *Anesthesiology*
1954 **107**, 264–272 (2007).
- 1955 191. Palanca, B. J. A., Avidan, M. S. & Mashour, G. A. Human neural correlates of
1956 sevoflurane-induced unconsciousness. *BJA Br. J. Anaesth.* **119**, 573–582 (2017).
- 1957 192. Golkowski, D. *et al.* Coherence of BOLD signal and electrical activity in the human
1958 brain during deep sevoflurane anesthesia. *Brain Behav.* **7**, 1–8 (2017).
- 1959 193. Golkowski, D. *et al.* Changes in Whole Brain Dynamics and Connectivity Patterns
1960 during Sevoflurane- and Propofol-induced Unconsciousness Identified by Functional
1961 Magnetic Resonance Imaging. *Anesthesiology* **130**, 898–911 (2019).
- 1962 194. Luppi, A. I. *et al.* Brain network integration dynamics are associated with loss and
1963 recovery of consciousness induced by sevoflurane. *Hum. Brain Mapp.* (2021)
1964 doi:10.1002/hbm.25405.
- 1965 195. Basso, L. *et al.* Antidepressant and neurocognitive effects of serial ketamine
1966 administration versus ECT in depressed patients. *J. Psychiatr. Res.* **123**, 1–8 (2020).
- 1967 196. Phillips, J. L. *et al.* Single and repeated ketamine infusions for reduction of suicidal
1968 ideation in treatment-resistant depression. *Neuropsychopharmacol. Off. Publ. Am. Coll.*
1969 *Neuropsychopharmacol.* **45**, 606–612 (2020).
- 1970 197. Corlett, P. R., Honey, G. D. & Fletcher, P. C. Prediction error, ketamine and psychosis:
1971 An updated model. *J. Psychopharmacol. (Oxf.)* **30**, 1145–1155 (2016).

- 1972 198. Moore, J. W. *et al.* Ketamine administration in healthy volunteers reproduces aberrant
1973 agency experiences associated with schizophrenia. *Cognit. Neuropsychiatry* **16**, 364–
1974 381 (2011).
- 1975 199. Studerus, E., Gamma, A. & Vollenweider, F. X. Psychometric evaluation of the altered
1976 states of consciousness rating scale (OAV). *PLoS ONE* **5**, (2010).
- 1977 200. Corlett, P. R. *et al.* Frontal responses during learning predict vulnerability to the
1978 psychotogenic effects of ketamine: Linking cognition, brain activity, and psychosis.
1979 *Arch. Gen. Psychiatry* **63**, 611–621 (2006).
- 1980 201. Marona-Lewicka, D. *et al.* Re-evaluation of lisuride pharmacology: 5-
1981 hydroxytryptamine_{1A} receptor-mediated behavioral effects overlap its other properties
1982 in rats. *Psychopharmacology (Berl.)* **164**, 93–107 (2002).
- 1983 202. Passie, T., Halpern, J. H., Stichtenoth, D. O., Emrich, H. M. & Hintzen, A. The
1984 pharmacology of lysergic acid diethylamide: A review. *CNS Neurosci. Ther.* **14**, 295–
1985 314 (2008).
- 1986 203. Kraehenmann, R. *et al.* Dreamlike effects of LSD on waking imagery in humans depend
1987 on serotonin 2A receptor activation. *Psychopharmacology (Berl.)* 1–16 (2017)
1988 doi:10.1007/s00213-017-4610-0.
- 1989 204. Tagliazucchi, E. *et al.* Increased Global Functional Connectivity Correlates with LSD-
1990 Induced Ego Dissolution. *Curr. Biol.* **26**, 1043–1050 (2016).
- 1991 205. Vollenweider, F. X., Vollenweider-Scherpenhuyzen, M. F., Bäbler, A., Vogel, H. & Hell,
1992 D. Psilocybin induces schizophrenia-like psychosis in humans via a serotonin-2 agonist
1993 action. *Neuroreport* **9**, 3897–3902 (1998).
- 1994 206. Passie, T., Seifert, J., Schneider, U. & Emrich, H. M. The pharmacology of psilocybin.
1995 *Addict. Biol.* **7**, 357–364 (2002).
- 1996 207. González-Maeso, J. *et al.* Hallucinogens recruit specific cortical 5-HT(2A) receptor-
1997 mediated signaling pathways to affect behavior. *Neuron* **53**, 439–452 (2007).

- 1998 208. McKenna, D. J., Repke, D. B., Lo, L. & Peroutka, S. J. Differential interactions of
1999 indolealkylamines with 5-hydroxytryptamine receptor subtypes. *Neuropharmacology* **29**,
2000 193–198 (1990).
- 2001 209. Halberstadt, A. L., Koedood, L., Powell, S. B. & Geyer, M. A. Differential contributions
2002 of serotonin receptors to the behavioral effects of indoleamine hallucinogens in mice. *J.*
2003 *Psychopharmacol. Oxf. Engl.* **25**, 1548–1561 (2011).
- 2004 210. Callaway, J. C. *et al.* Pharmacokinetics of Hoasca alkaloids in healthy humans. *J.*
2005 *Ethnopharmacol.* **65**, 243–256 (1999).
- 2006 211. Fontanilla, D. *et al.* The hallucinogen N,N-dimethyltryptamine (DMT) is an endogenous
2007 sigma-1 receptor regulator. *Science* **323**, 934–937 (2009).
- 2008 212. McKenna, D. J., Towers, G. H. & Abbott, F. Monoamine oxidase inhibitors in South
2009 American hallucinogenic plants: tryptamine and beta-carboline constituents of
2010 ayahuasca. *J. Ethnopharmacol.* **10**, 195–223 (1984).
- 2011 213. Buckholtz, N. S. & Boggan, W. O. Monoamine oxidase inhibition in brain and liver
2012 produced by β -carbolines: structure-activity relationships and substrate specificity.
2013 *Biochem. Pharmacol.* **26**, 1991–1996 (1977).
- 2014 214. Mckenna, D., Riba, J., Mckenna, D. & Riba, J. New World Tryptamine Hallucinogens
2015 and the Neuroscience of Ayahuasca. *Curr Top. Behav Neurosci* **36**, 283–311 (2016).
- 2016 215. Ghahremani, D. G. *et al.* Effect of Modafinil on Learning and Task-Related Brain
2017 Activity in Methamphetamine-Dependent and Healthy Individuals.
2018 *Neuropsychopharmacology* **36**, 950–959 (2011).
- 2019 216. Ishizuka, T., Murotani, T. & Yamatodani, A. Modanifil activates the histaminergic
2020 system through the orexinergic neurons. *Neurosci. Lett.* **483**, 193–196 (2010).
- 2021 217. Volkow, N. D. *et al.* Effects of Modafinil on Dopamine and Dopamine Transporters in
2022 the Male Human Brain: Clinical Implications. *JAMA J. Am. Med. Assoc.* **301**, 1148–
2023 1154 (2009).
- 2024 218. Gass, J. T. & Foster Olive, M. Glutamatergic substrates of drug addiction and
2025 alcoholism. *Biochem. Pharmacol.* **75**, 218–265 (2008).

- 2026 219. Wisor, J. P. *et al.* Dopaminergic role in stimulant-induced wakefulness. *J. Neurosci. Off.*
2027 *J. Soc. Neurosci.* **21**, 1787–1794 (2001).
- 2028 220. Madras, B. K. *et al.* Modafinil Occupies Dopamine and Norepinephrine Transporters in
2029 Vivo and Modulates the Transporters and Trace Amine Activity in Vitro. *J. Pharmacol.*
2030 *Exp. Ther.* **319**, 561–569 (2006).
- 2031 221. Cera, N., Tartaro, A., Sensi, S. L. & Jan Stam, C. Modafinil Alters Intrinsic Functional
2032 Connectivity of the Right Posterior Insula: A Pharmacological Resting State fMRI Study.
2033 *PLOS ONE* (2014) doi:10.1371/journal.pone.0107145.
- 2034 222. Hannestad, J. *et al.* Clinically relevant doses of methylphenidate significantly occupy
2035 norepinephrine transporters in humans in vivo. *Biol. Psychiatry* **68**, 854–860 (2010).
- 2036 223. Rowley, H. L. *et al.* Differences in the neurochemical and behavioural profiles of
2037 lisdexamfetamine methylphenidate and modafinil revealed by simultaneous dual-probe
2038 microdialysis and locomotor activity measurements in freely-moving rats. *J.*
2039 *Psychopharmacol. Oxf. Engl.* **28**, 254–269 (2014).
- 2040 224. Koda, K. *et al.* Effects of acute and chronic administration of atomoxetine and
2041 methylphenidate on extracellular levels of noradrenaline, dopamine and serotonin in the
2042 prefrontal cortex and striatum of mice. *J. Neurochem.* **114**, 259–270 (2010).
- 2043 225. Williard, R. L., Middaugh, L. D., Zhu, H.-J. B. & Patrick, K. S. Methylphenidate and its
2044 ethanol transesterification metabolite ethylphenidate: brain disposition, monoamine
2045 transporters and motor activity. *Behav. Pharmacol.* **18**, 39–51 (2007).
- 2046 226. Markowitz, J. S., DeVane, C. L., Pestreich, L. K., Patrick, K. S. & Muniz, R. A
2047 comprehensive in vitro screening of d-, l-, and dl-threo-methylphenidate: an exploratory
2048 study. *J. Child Adolesc. Psychopharmacol.* **16**, 687–698 (2006).
- 2049 227. Volkow, N. D., Fowler, J. S., Wang, G., Ding, Y. & Gatley, S. J. Mechanism of action of
2050 methylphenidate: insights from PET imaging studies. *J. Atten. Disord.* **6 Suppl 1**, S31-
2051 43 (2002).
- 2052 228. Volkow, N. D. *et al.* Dopamine transporter occupancies in the human brain induced by
2053 therapeutic doses of oral methylphenidate. *Am. J. Psychiatry* **155**, 1325–1331 (1998).

- 2054 229. Whitfield-Gabrieli, S. & Nieto-Castanon, A. Conn: A Functional Connectivity Toolbox for
2055 Correlated and Anticorrelated Brain Networks. *Brain Connect.* **2**, 125–141 (2012).
- 2056 230. Power, J. D., Barnes, K. A., Snyder, A. Z., Schlaggar, B. L. & Petersen, S. E. Spurious
2057 but systematic correlations in functional connectivity MRI networks arise from subject
2058 motion. *NeuroImage* **59**, 2142–2154 (2012).
- 2059 231. Behzadi Y, Restom K, Liau J, & Liu TT. A component based noise correction method
2060 (CompCor) for BOLD and perfusion based fMRI. *NeuroImage* **37**, 90–101 (2007).
- 2061 232. Andellini, M., Cannatà, V., Gazzellini, S., Bernardi, B. & Napolitano, A. Test-retest
2062 reliability of graph metrics of resting state MRI functional brain networks: A review. *J.*
2063 *Neurosci. Methods* **253**, 183–192 (2015).
- 2064 233. Lydon-Staley, D. M., Ciric, R., Satterthwaite, T. D. & Bassett, D. S. Evaluation of
2065 confound regression strategies for the mitigation of micromovement artifact in studies of
2066 dynamic resting-state functional connectivity and multilayer network modularity. *Netw.*
2067 *Neurosci.* **3**, 427–454 (2019).
- 2068 234. Power, J. D. *et al.* Methods to detect, characterize, and remove motion artifact in
2069 resting state fMRI. *NeuroImage* **84**, 320–341 (2014).
- 2070 235. Murphy, K. & Fox, M. D. Towards a consensus regarding global signal regression for
2071 resting state functional connectivity MRI. *NeuroImage* **154**, 169–173 (2017).
- 2072 236. Tanabe, S. *et al.* Altered Global Brain Signal during Physiologic, Pharmacologic, and
2073 Pathologic States of Unconsciousness in Humans and Rats. *Anesthesiology* 1392–
2074 1406 (2020) doi:10.1097/ALN.0000000000003197.
- 2075 237. Thompson, P. M. *et al.* ENIGMA and global neuroscience: A decade of large-scale
2076 studies of the brain in health and disease across more than 40 countries. *Transl.*
2077 *Psychiatry* **10**, 1–28 (2020).
- 2078
2079
2080